



Dating of granite-related tin mineralisation at Quy Hop, Vietnam: Constraints from zircon and cassiterite U–Pb and muscovite $^{40}\text{Ar}/^{39}\text{Ar}$ geochronology



Dinh Cong Bui ^{a,b,c}, Hua-Ning Qiu ^{a,b,*}, Xuan Dac Ngo ^d, Xiu-Juan Bai ^{a,b,*}, Yang Wu ^a

^a Key Laboratory of Tectonics and Petroleum Resources, China University of Geosciences, Ministry of Education, Wuhan 430074, China

^b School of Earth Resources, China University of Geosciences, Wuhan 430074, China

^c Department of Mineral Resources, Vietnam Institute of Geosciences and Mineral Resources, Hanoi, Viet Nam

^d Department of Mineral Resource Prospecting and Exploration, Hanoi University of Mining and Geology, Hanoi, Viet Nam

ARTICLE INFO

Keywords:

Zircon U–Pb dating
Cassiterite U–Pb dating
 $^{40}\text{Ar}/^{39}\text{Ar}$ dating
Quy Hop tin deposit
Ban Chieng granite
North Central Vietnam

ABSTRACT

Quy Hop is an important tin mining district in the North Central Coast province of Vietnam. The exposed magmatic plutons include Late Oligocene – Early Miocene granitoid and Middle Triassic granitic gneiss. Tin mineralisation in the area is spatially associated with biotite granite of the Ban Chieng Complex. Quartz vein-type and greisen-type tin ores occur in quartz-sericite-graphite schist of the Ordovician-Silurian Song Ca Formation and the greisenised granite of the Late Oligocene Ban Chieng Complex, respectively. The lack of accurate geochronological dates for the tin deposits and spatially associated granitic rocks limits our understanding of the genetic relationship between tin mineralisation and granitoid intrusions. In this study, granitic zircon and cassiterite laser ablation and inductively coupled plasma mass spectrometry U–Pb and muscovite $^{40}\text{Ar}/^{39}\text{Ar}$ dating techniques were applied to address this lack of understanding. Granitic zircon U–Pb dating of two biotite granite samples obtained from Ban Chieng yielded intersection ages of 26.65 ± 0.33 and 23.89 ± 0.15 Ma, interpreted here as representative igneous emplacement ages. Cassiterite U–Pb analyses yielded $^{207}\text{Pb}/^{206}\text{Pb}$ – $^{238}\text{U}/^{206}\text{Pb}$ intersection ages of 26.81 ± 1.92 Ma for the quartz vein ore from Suoi Bac and 23.23 ± 0.89 Ma for greisen ore from Ban Ngoc. Muscovite $^{40}\text{Ar}/^{39}\text{Ar}$ laser step heating of the greisen ore yielded a plateau age of 23.87 ± 0.14 Ma and a corresponding inverse isochron age of 23.85 ± 0.16 Ma. These geochronological results strongly suggest that tin mineralisation at Quy Hop occurred in the period between 26 and 23 Ma and, therefore, is closely genetically related to the Late Palaeogene granites of the Ban Chieng Complex. The exploration implication of the new age data is considerable, indicating that biotite granite intrusions may be favourable for tin mineralisation across the entire Phu Hoat Terrane.

1. Introduction

Accurately determining the age of a formation is crucial to the study of ore deposits. For example, geochronology plays a major role in determining temporal and genetic relationships between igneous intrusions and associated hydrothermal ores. Modern techniques used to determine the formation ages of rocks and ores include U–Pb, $^{40}\text{Ar}/^{39}\text{Ar}$, Re–Os, Rb–Sr, and Sm–Nd dating (Nakai et al., 1993; Bai et al., 2013; Zhang et al., 2014; Zhang et al., 2015; Zhang et al., 2019b).

Muscovite $^{40}\text{Ar}/^{39}\text{Ar}$ dating is particularly effective at determining hydrothermal mineralisation ages with high precision (Hu et al., 2012; Bai et al., 2013; Chen et al., 2014; Zhang et al., 2014; Zhang et al., 2015).

Additionally, U-bearing minerals, such as zircon, monazite, titanite, rutile, and uraninite, have been successfully used in laser ablation and inductively coupled plasma mass spectrometry (LA-ICP-MS) U–Pb dating, yielding precise ages for magmatic, hydrothermal, and metamorphic rocks and ore deposits (Machado and Simonetti, 2001; Simonetti et al., 2006; Bracciali et al., 2013; Zong et al., 2015). Cassiterite is the predominant tin-bearing ore found in hydrothermal veins, pegmatites, and greisen associated with granite intrusions (Taylor, 1979; Lehmann, 1982). It belongs to the rutile group (M^{4+}O_2) and typically has a high U and low Pb content (Gulson and Jones, 1992; Zack and Kooijman, 2017). Thus, cassiterite is considered a suitable mineral for U–Pb dating of tin deposits (Zhang et al., 2015; Zhang et al., 2020).

* Corresponding authors at: Key Laboratory of Tectonics and Petroleum Resources, China University of Geosciences, Ministry of Education, Wuhan 430074, China.
E-mail addresses: huaningqiu@cug.edu.cn (H.-N. Qiu), xiuj.bai@cug.edu.cn (X.-J. Bai).

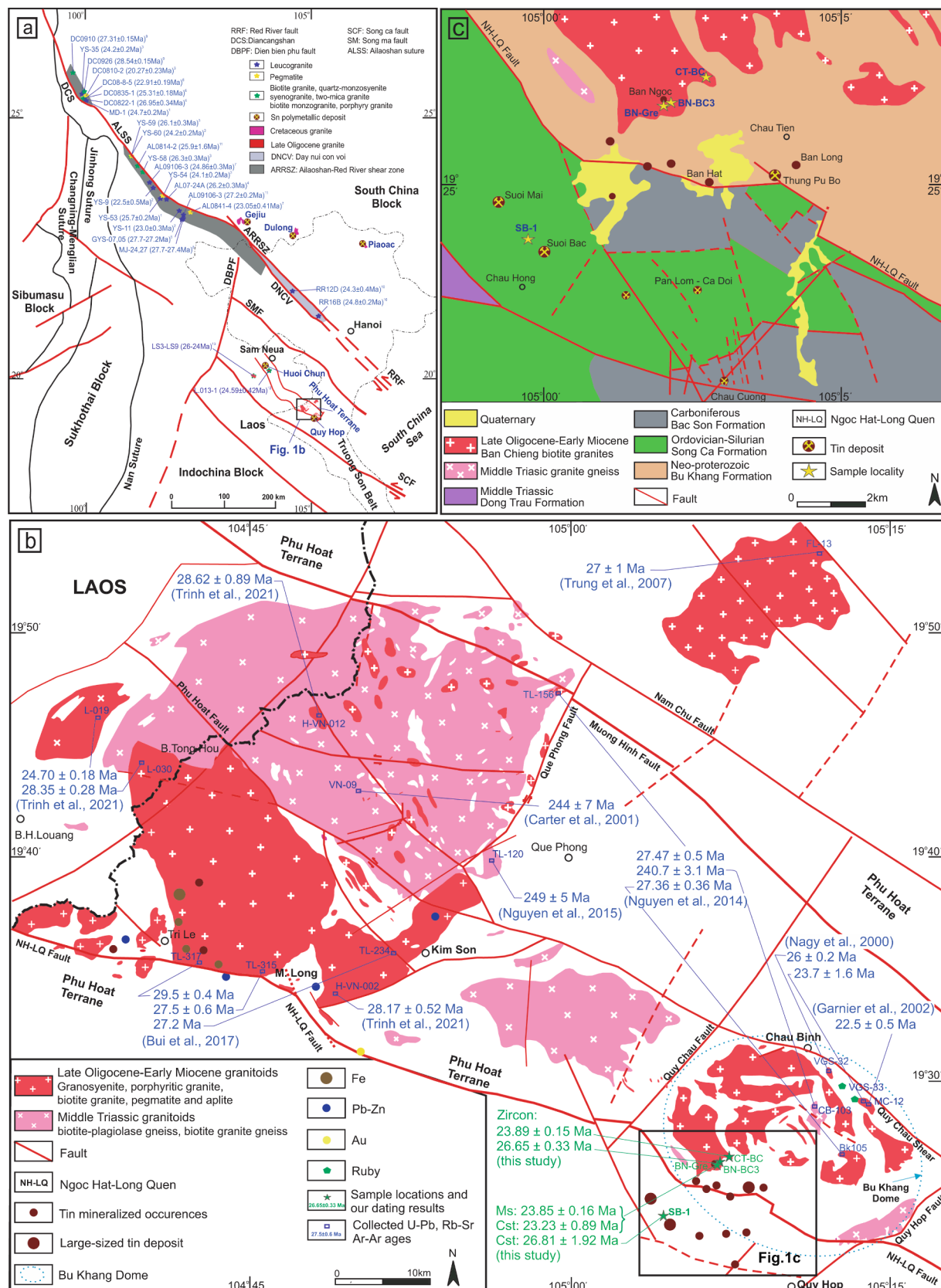


Fig. 1. (a) Tectonic map of Indochina, adapted from Zhang and Schärer (1999) and Tang et al. (2013); (b) sketch map illustrating the spatial distribution of magmatic rocks in the Phu Hoat Terrane, adapted from Bui et al. (2017); and (c) regional geological map of Quy Hop. Geochronology data are sourced from [1] Zhang and Schärer (1999); [2] Schärer et al. (1990); [3] Schärer et al. (1994); [4] Searle et al. (2010); [5] He et al. (2019); [6] Cao et al. (2011); [7] Liu et al. (2015); [8] He et al. (2020); [9] Chen et al. (2017); [10] Wang et al. (1998); [11] Tang et al. (2013); [12] Trinh et al. (2021); and [13] Wang et al. (2019).

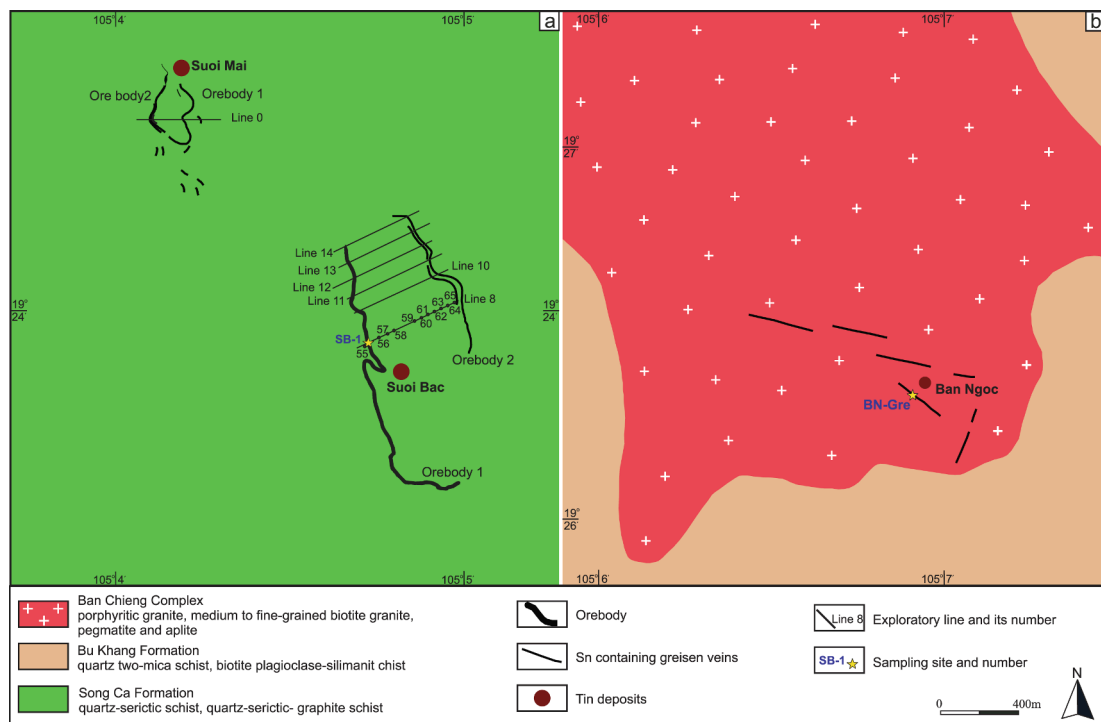


Fig. 2. Simplified geological map of Quy Hop: (a) Suoi Bac with exploration lines labelled, and (b) Ban Ngoc.

Over the years, different cassiterite U–Pb dating techniques have been developed to determine the age of tin mineralisation events (Gulson and Jones, 1992; Liu et al., 2007; Yuan et al., 2008; Zhang et al., 2014; Li et al., 2016; Zhang et al., 2017a; Chen et al., 2018; Mao et al., 2020). For example, Yuan et al. (2011) developed the in situ LA-ICP-MS U–Pb cassiterite dating technique, which is commonly used to rapidly determine the ages of tin deposits (Chen et al., 2014; Zhang et al., 2015; Neymark et al., 2018; Zhang et al., 2020).

The Quy Hop District, located in the north-western Nghe An Province in the North Central Coast of Vietnam, is an important tin mineralisation area of the Phu Hoat Terrane in the central Truong Son Belt, which belongs to the Indochina Block tin metallogenic province of the South-east Asian Tin Belt (Duong et al., 1983; Hutchison, 1984). Tin deposits at Quy Hop are the result of quartz vein-type and greisen-type mineralisation. Quartz vein deposits are the predominant type and occur in quartz-sericite-graphite schist. A current lack of precise geochronological age data poses a challenge in determining the relationship between tin mineralisation and local magmatic intrusive rocks. Previous studies have focused mainly on granitic rocks, using zircon U–Pb, whole rock Rb–Sr, and biotite K–Ar and Ar–Ar dating techniques (Lepvrier et al., 1997; Jolivet et al., 1999; Nagy et al., 2000; Garnier et al., 2002; Trung et al., 2007; Nguyen et al., 2014; Bui et al., 2017), yielding ages ranging from 29.5 to 22.1 Ma. However, the genetic relationship between hydrothermal tin mineralisation and spatially-associated granites at Quy Hop remains ambiguous. To better understand this genetic relationship, we selected muscovite and cassiterite from tin ores and zircon from granitic rocks for geochronology using $^{40}\text{Ar}/^{39}\text{Ar}$ laser step-heating and *in situ* LA-ICP-MS U–Pb dating to determine the ages of ore formation and granite emplacements at Quy Hop.

2. Geological setting

2.1. Regional geology

Phu Hoat is a metamorphic terrane with a NW-SE orientation extending from Vietnam to Laos, located between the Song Ca fault to the north-east, the Song Ma fault to the south-west, and the Sam Neua

zone to the south-east (Fig. 1a) (Lepvrier et al., 1997; Jolivet et al., 2001) and situated in the central Truong Son Belt (Lepvrier et al., 1997; Lepvrier et al., 2004; Tran et al., 2008). Truong Son is an important tectonic and metallogenic belt in the Indochina Block (Lepvrier et al., 1997; Lepvrier et al., 2004; Tran et al., 2008; Roger et al., 2012; Liu et al., 2012a) playing host to the mineralisation of several rare metal ores, including tin, iron, lead, zinc, copper, gold, and silver (Tran et al., 2009; Kamvong et al., 2014; Manaka et al., 2014; Zaw et al., 2014; Shi et al., 2015; Hou et al., 2019).

Consisting of a crystalline block of Precambrian metamorphic rocks, the Phu Hoat Terrane has been identified by many different names: Tectonic Arc (Fromaget, 1941), Structural-Facial Zone (Dovjikov et al., 1965), Central Massif (Bach, 1969), Late Hercynian Fold Zone (Tran et al., 1986), Phu Hoat Massif (Lepvrier et al., 1997) and Late Neoproterozoic-Early Palaeozoic Microcontinent (Tran et al., 2020). The metasedimentary and sedimentary rocks in the Phu Hoat Terrane comprise Proterozoic, Palaeozoic, and Mesozoic formations, which were intruded by Triassic and Paleogenic granitic rocks (Jolivet et al., 1999). The metasedimentary and sedimentary rock sequences are divided into four stratigraphic units: the Bu Khang Formation (Neoproterozoic schist), Song Ca Formation (Ordovician-Silurian schist), Bac Son Formation (Carboniferous limestone), and Dong Trau Formation (Middle Triassic tuffaceous sandstone, tuffaceous siltstone and rhyolite) (Dovjikov et al., 1965; Bach et al., 2001). Emplacement of granitoid intrusions mainly occurred during Late Oligocene – Early Miocene and Middle Triassic times with intrusions of these ages widespread in the Phu Hoat Terrane, including granosyenite, porphyritic granite, biotite granite, pegmatite, and aplite belonging to the Late Oligocene-Early Miocene Ban Chieng Complex and unnamed Middle Triassic biotite-plagioclase and biotite granitic gneiss complexes (Nagy et al., 2000; Bui et al., 2017).

Situated within the Phu Hoat Terrane, the Bu Khang Dome is an extensional structure dating to the Oligocene – Miocene (Jolivet et al., 1999), with evidence of left-lateral ductile deformation along the Ailaoshan–Red River shear zone (ASRR) (Jolivet et al., 1999; Nagy et al., 2000). The ASRR is a large-scale NW-SE trending shear zone, located to the east of the Ailaoshan suture (Deng et al., 2015), which plays an

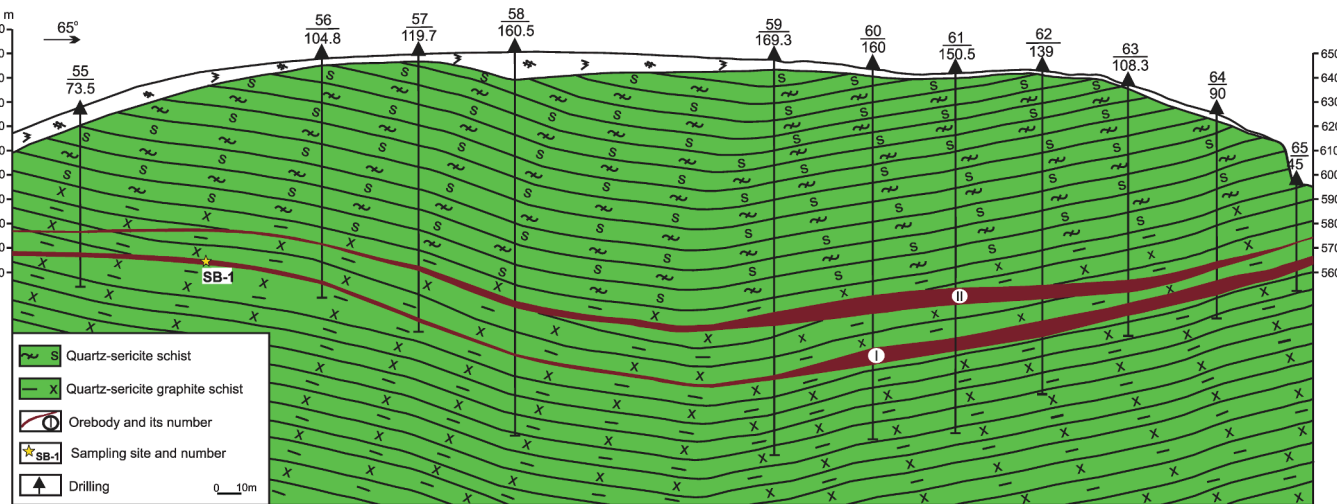


Fig. 3. Geological cross section along exploration line No. 8 at Suoi Bac (see Fig. 2a), adapted from Nguyen (2012).

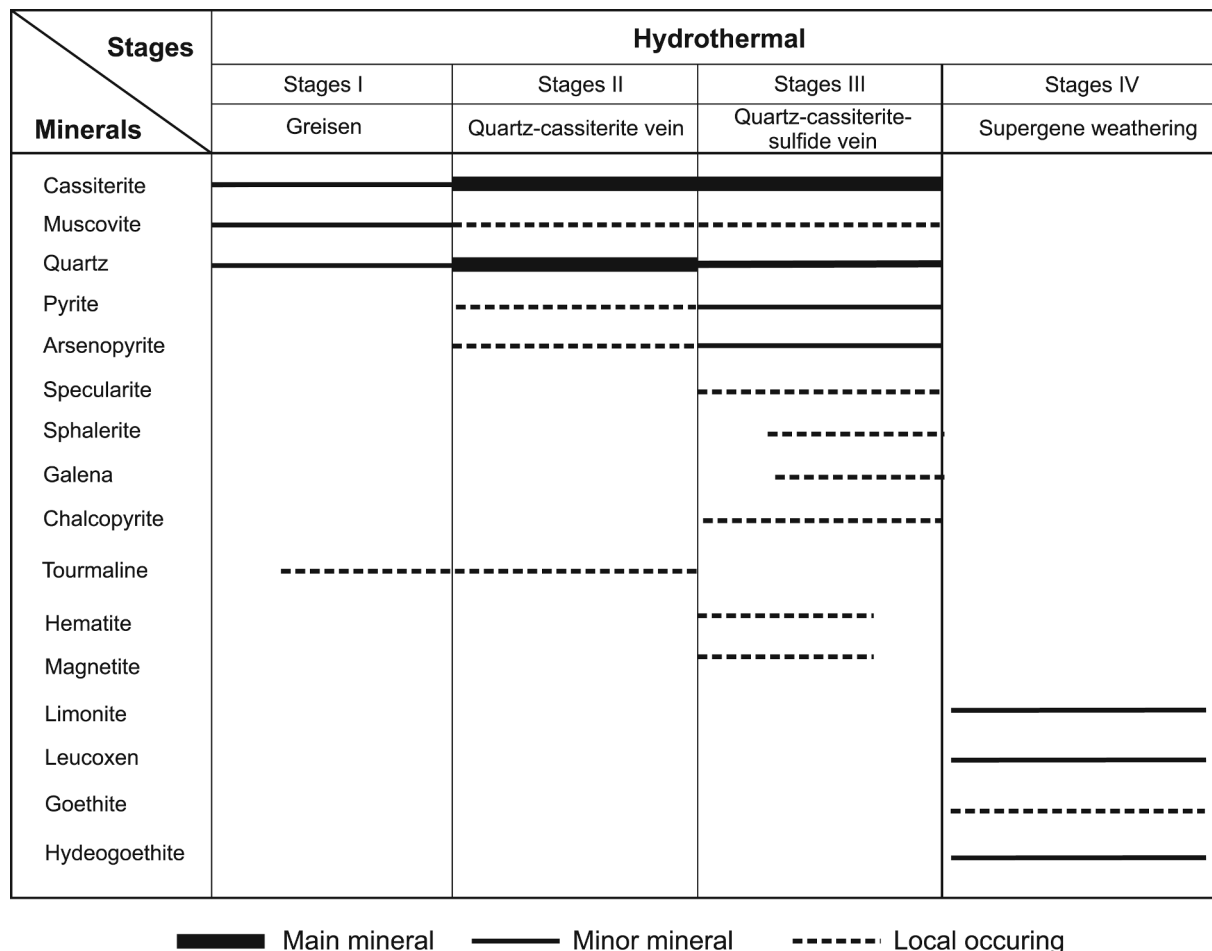


Fig. 4. Paragenetic sequence of ore and gangue minerals at the Suoi Bac tin deposit (Quy Hop), adapted from Le (2015).

important role in Cenozoic Cu-Mo-Au mineralisation (Xu et al., 2012; Deng et al., 2015; Duong et al., 2021).

Middle Triassic granitic gneiss has yielded sensitive high resolution ion microprobe (SHRIMP) U-Pb zircon ages of 244 ± 7 Ma (Carter et al., 2001) and 249–241 Ma (Nguyen et al., 2014; Nguyen et al., 2015). The Ban Chieng Complex, composed of granosyenite, porphyritic granite, and biotite granite, yielded SHRIMP U-Pb zircon

ages of 29.5–27.4 Ma (Bui et al., 2017), monazite and zircon U-Pb ages of 26.0–23.7 Ma (Nagy et al., 2000), zircon LA-ICP-MS U-Pb ages of 28.62–24.70 Ma (Trinh et al., 2021), whole rock Rb-Sr isochron ages of 27 ± 1 Ma, and biotite K-Ar isochron ages of 24.5 ± 0.6 Ma (Trung et al., 2007). Biotite found in granitic pegmatite and granite rocks yielded $^{40}\text{Ar}/^{39}\text{Ar}$ ages of 27.3–22.1 Ma (Fig. 1b) (Lepvrier et al., 1997; Jolivet et al., 1999; Garnier et al., 2002).

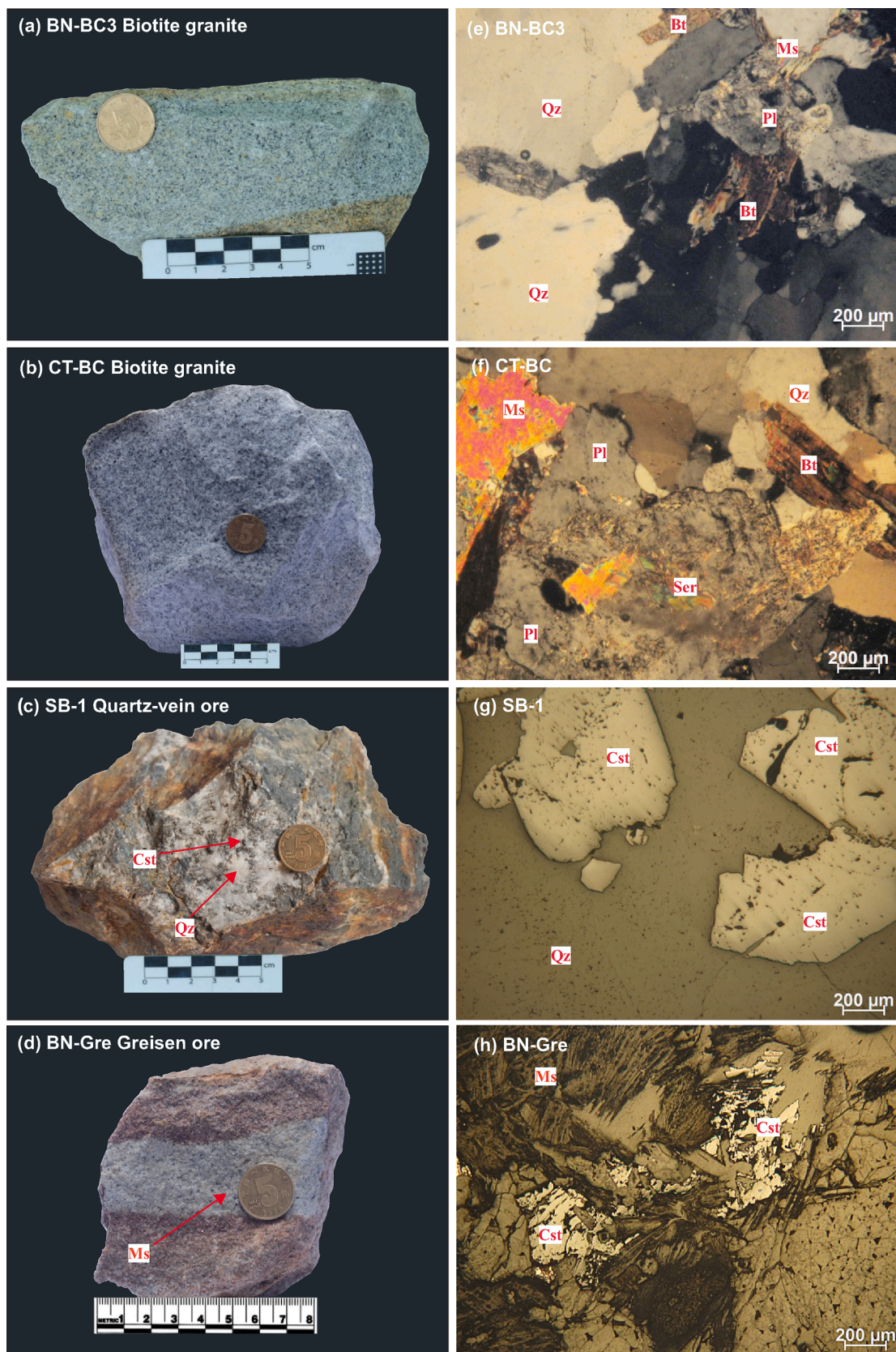


Fig. 5. Photographs (a–d) and photomicrographs (e–h) of granitic rocks and the predominant types of tin ores from Quy Hop: (a) fine-grained biotite granite; (b) medium-grained biotite granite; (c) quartz vein ore from Suoi Bac; (d) greisen ore from Ban Ngoc; (e) fine-grained biotite granite; (f) medium-grained biotite granite; (g) quartz vein ore showing the euhedral granular cassiterite; and (h) greisen ore showing plagioclase (Pl), cassiterite (Cst), Sericite (Ser), quartz (Qz), muscovite (Ms), and biotite (Bt).

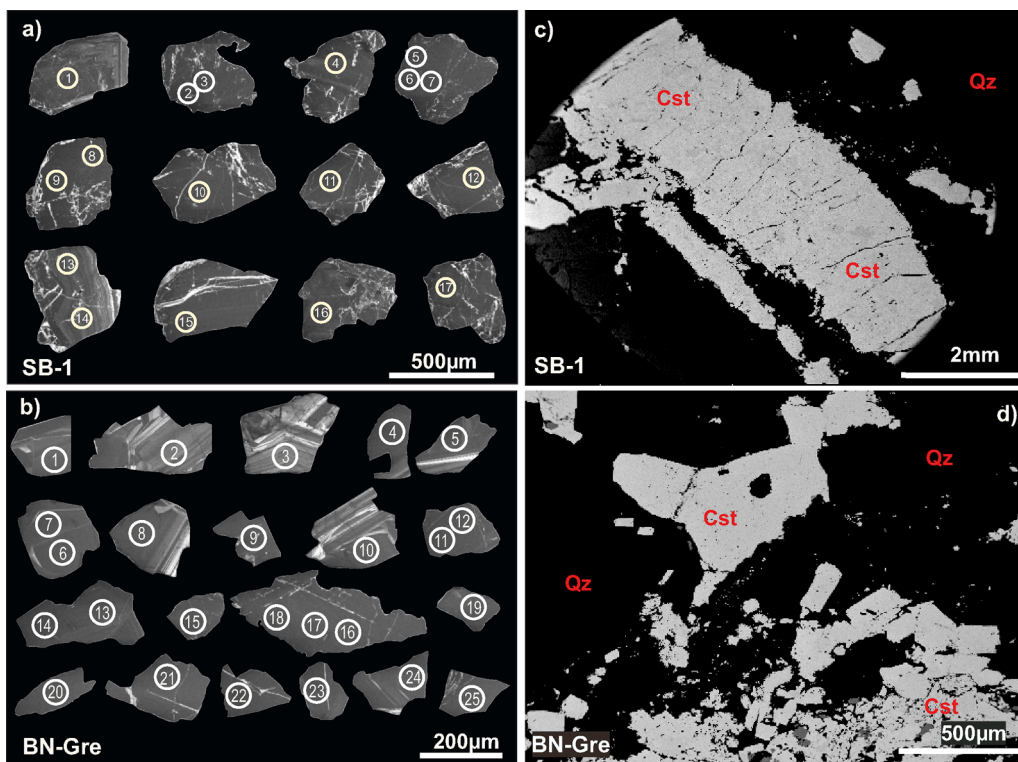


Fig. 6. (a, b) Cathodoluminescence (CL) and (c, d) backscattered electron (BSE) images of cassiterite (Cst) and quartz (Qz) obtained from the Suoi Bac and Ban Ngoc deposits. Ellipses indicate in situ locations of LA-ICP-MS analysis of U/Pb isotopes.

2.2. Ore deposit geology and granite petrology

Quy Hop is located in the south-eastern section of the Phu Hoat Terrane and forms part of the Bu Khang Dome (Fig. 1b and c) (Lepvrier et al., 1997; Jolivet et al., 1999; Nagy et al., 2000). The area mostly coincides with the Ngoc Hat-Long Quen fault and several other SE-NW and SW-NE faults (Fig. 1c). The Ngoc Hat-Long Quen fault, the most prominent in the area, has a SE-NW orientation but has been shifted to the south-west by younger NE-SW-trending faults.

Quy Hop has one of the largest tin reserves in Vietnam. Cassiterite dispersion haloes were first reported by Dovjikov et al. (1965). A series of subsequent studies have revealed several tin deposits at Quy Hop in the form of both quartz veins and greisen. The quartz vein and greisen ore samples used in this study were collected from the Suoi Bac and Ban Ngoc tin deposits, respectively (Fig. 1c).

Tin mineralisation in Quy Hop occurs mainly in Ordovician-Silurian metamorphic rocks of the Song Ca Formation and fractured zones cutting this formation. The metamorphic host rocks are composed of quartz-biotite schist, quartz-two-mica schist, garnet-bearing two-mica quartz schist, quartz-sericite schist, and quartz-sericite-graphite schist. These rocks are significantly weathered and mottled, yellowish and brownish grey in colour, and have a combined thickness of 450 m. The tin ore mainly occurs in dark grey quartz-sericite-graphite schist, which is altered by silicification and tourmalinisation, with quartz comprising 30–35%, sericite 40–70%, and graphite 3–10% of the rock mass.

Tin mineralisation is controlled by the SE-NW-striking Ngoc Hat-Long Quen fault and fracture systems (Fig. 1c), which served as major fluid pathways. The surrounding rocks were altered and fractured by hydrothermal activity. The tin orebodies in Quy Hop are mainly hosted in the metamorphosed country rocks of the Song Ca Formation (Fig. 2a).

The Suoi Bac deposit in the Chau Hong area, located in the south-western portion of the Phu Hoat Terrane, is the largest deposit in Quy Hop (Fig. 1b), with a Sn reserve of 5,806 tons and an average Sn grade of 0.59%. The ore bodies occur along a SE-NW line within the foliations of quartz-sericite-graphite schist in an eroded syncline (Fig. 3). Ore body

No. 1 is the largest in this deposit, over 800 m long, 4.2 m thick, and with a high Sn grade of 5.71%. The predominant ore minerals comprise cassiterite, pyrite, and arsenopyrite, while minor minerals include haematite, goethite, and limonite. Gangue minerals mainly include quartz, graphite, biotite, tourmaline, and sericite (Fig. 4 and Fig. 5). Cassiterite occurs in the form of euhedral and anhedral grains with a diameter of 200–600 µm (Fig. 6a), commonly found in quartz veins and surrounding altered zones (Fig. 5c). The hydrothermal alteration of these rocks entailed processes of sericitisation, silicification, tourmalinisation, and graphitisation. In terms of field evidence and petrographic observations, the mineral paragenesis of Suoi Bac can be divided into four stages (Fig. 4): greisen (Stage I), quartz-cassiterite vein (Stage II), quartz-cassiterite-sulphide vein (Stage III), and supergene weathering (Stage IV). Cassiterite was mainly formed at Stage II and III, with a small amount forming at Stage I with muscovite (Fig. 5c-h). Some sulphides (arsenopyrite and pyrite) occurred in the quartz veins at Stage III (Fig. 5c).

In Ban Ngoc, tin-bearing greisen occurs in biotite granite of the Late Oligocene – Early Miocene Ban Chieng Complex (Fig. 2b). The lenticular greisen bodies developed along a SW-NE trending line, with discontinuous lengths of approximately 100–400 m and a low Sn grade of 0.15%. Cassiterite, the tin ore found within greisen bodies, occurs as fine-grained (50–250 µm in diameter) anhedral and subhedral shapes (Fig. 6b). Gangue minerals found in greisen include quartz, muscovite, fluorite, arsenopyrite, and pyrite.

Exposed rock formations at Quy Hop include the following: (1) the Neoproterozoic Bu Khang Formation, comprising quartz-biotite, biotite-plagioclase-sillimanite, and garnet-bearing quartz two-mica schists; (2) the Ordovician Song Ca Formation, comprising quartz-sericite, quartz-sericite-graphite, and quartz two-mica schists; (3) the Carboniferous Bac Son Formation, comprising limestone; and (4) the Triassic Dong Trau Formation, comprising tuffaceous sandstone, tuffaceous siltstone, and rhyolite (Fig. 1c) (Bach et al., 2001). Ban Chieng biotite granite is exposed in the north-eastern portion of the Suoi Bac deposit (Fig. 1b, c) and the Bu Khang Dome, cutting through the metamorphic schists of the



Fig. 7. Cathodoluminescence (CL) images of zircon obtained from biotite granite. Circled data indicate locations and ages determined via LA-ICP-MS dating.

Neoproterozoic Bu Khang Formation (Lepvrier et al., 1997; Jolivet et al., 1999; Nagy et al., 2000). Biotite granite is light grey to grey in colour and fine- to medium-grained in texture (Fig. 5a, b). Its constituent minerals include K-feldspar, plagioclase, quartz, and biotite. Plagioclase and K-feldspar are subhedral to anhedral in shape and have been altered over time to sericite and kaolinite, respectively (Fig. 5e, f). Quartz is the most abundant of these minerals, with a typical anhedral structure (Fig. 5e, f). Lastly, biotite is anhedral and blackish brown (Fig. 5f). Accessory minerals comprise zircon, monazite, and some opaque minerals.

3. Sampling and analytical methods

3.1. Sample collection

Granite and cassiterite were collected from Quy Hop for chronologic study. Two biotite granite samples (BN-BC3 and CT-BC) were collected for zircon LA-ICP-MS U–Pb dating from different outcrops of the Ban Chiang Complex at Ban Ngoc and Chau Tien, respectively (Fig. 1c). Sample BN-BC3 comprised fine-grained biotite granite, grey in colour and massive in structure (Fig. 5a), which was composed of K-feldspar (8–10%), plagioclase (35–40%), quartz (25–35%), biotite (5–10%) (Fig. 5e). Accessory minerals (3–5%) included zircon, monazite, and opaque minerals. Sample CT-BC comprised light grey biotite granite with a medium-grained texture (Fig. 5b), containing K-feldspar (5–10%), plagioclase (40–45%), quartz (45–55%), biotite (5–8%), muscovite (1–3%) (Fig. 5f), and accessory minerals including zircon, apatite, and monazite.

Two ore samples were selected for cassiterite LA-ICP-MS U–Pb dating. Sample SB-1 was obtained from quartz vein ore body No. 1 in Suoi Bac (Fig. 2a), with yellow to dark brown cassiterite grains (Fig. 5c), and sample BN-Gre was obtained from the greisen ore in Ban Ngoc (Fig. 2b), which contained dark brown cassiterite, greasy quartz, and minor muscovite (Fig. 5d).

3.2. Muscovite $^{40}\text{Ar}/^{39}\text{Ar}$ dating

A muscovite sample was separated from sample BN-Gre. Pure muscovite grains were carefully handpicked under a binocular microscope, cleaned in an ultrasonic bath with deionised water, and dried in an oven at 100 °C. The muscovite grains were wrapped with aluminium foil and irradiated for 20 h in a newly built China Mianyang Research Reactor (CMRR). The ZBH-25 biotite sample obtained from Fangshan granodiorite (132.7 ± 1.2 Ma) was used to monitor the neutron flux with a K content of 7.579% (Wang, 1983). The $^{40}\text{Ar}/^{39}\text{Ar}$ laser step heating process was carried out at the Key Laboratory of Tectonics and Petroleum Resources, China University of Geosciences, Ministry of Education, using a multi-collector ARGUS VI® noble gas mass spectrometer. Detailed analytical procedures were described by Bai et al. (2018b). To calculate the $^{40}\text{Ar}/^{39}\text{Ar}$ age, a ^{40}K decay constant of $5.530 \times 10^{-10} \text{ a}^{-1}$ (Renne et al., 2011) and modern atmospheric ratio of 298.56

(Lee et al., 2006) were adopted. The $^{40}\text{Ar}/^{39}\text{Ar}$ data were calculated and plotted using ArArCALC 2.5.2b software (Koppers, 2002).

3.3. Zircon LA-ICP-MS U–Pb dating

Zircons were separated from crushed granite samples in a steel jaw mill using magnetic and heavy liquid separation techniques. Pure zircon grains were subsequently hand-selected under a binocular microscope, mounted on epoxy resin disks, and polished. Their internal morphology and texture were recorded using cathodoluminescence (CL) prior to U–Pb isotopic analysis.

Zircon U–Pb dating of two samples (BN-BC3 and CT-BC) was carried out using LA-ICP-MS at the Wuhan Sample Solution Analytical Technology Co., Ltd. Detailed analytical procedures, operating conditions, and data reduction methods were described by Zong et al. (2017). A Coherent GeolasPro 193 nm laser ablation (LA) system was used for laser sampling, and ion signal intensities were determined using an Agilent 7700e inductively coupled plasma-mass spectrometer (ICP-MS). During the LA process, He was used as the carrier gas and Ar as the compensation gas to adjust sensitivity. The two gasses were mixed using a T-connector before entering the ICP-MS. The spot size and frequency of all zircon data zircon were set to 32 μm and 5 Hz, respectively. During the analysis, the standard zircon reference materials 91500 (1062 ± 4 Ma), NIST SRM 610 and GJ-1 (610.0 ± 1.7 Ma) were used as external and secondary standards for U–Pb dating (Wiedenbeck et al., 1995; Wiedenbeck et al., 2004; Elhlou et al., 2006). The zircon standard 91500 was used to correct inter-element fractionation and was analysed twice after every six unknown sample analyses (i.e., twice 91500 – six unknown samples – twice 91500 – six unknown samples ...). That is, time-dependent drifts of U–Th–Pb isotopic ratios were corrected using a linear interpolation (with time) based on the variations of zircon 91500 (Liu et al., 2010).

The preferred U, Th, and Pb isotopic ratios of zircon 91500 are based on Wiedenbeck et al. (1995). Each time-resolved analysis included approximately 20–30 s of blank signal, followed by 50 s of data acquisition from the sample. Offline selection and integration of background and analytic signals, time-drift correction, and quantitative calibration of trace element analyses and zircon U–Pb dating were performed using ICPMSDataCal 10.9 software (Liu et al., 2010). The zircon U–Pb age calculation of sample CT-BC and subsequent plotting of Concordia were done both online and offline, using the software IsoplotR (Vermeesch, 2018) and Isoplot 3.7 (Ludwig, 2003), respectively.

3.4. Cassiterite LA-ICP-MS U–Pb dating

Cassiterite samples were crushed and sieved through 40–60 meshes, after which the cassiterite grains were separated using heavy liquid and magnetic separation techniques. The grains were carefully checked under a binocular microscope for surface alteration, inclusions and fractures, using an external standard cassiterite sample (AY-4) with an isotope dilution-thermal ionization mass spectrometry U–Pb age of

Table 1

LA-ICP-MS U–Pb dating results for zircon samples from biotite granites.

Sample spots	Th ppm	U ppm	Th/U	Isotopic ratios								Ages (Ma)							
				$^{207}\text{Pb}/^{206}\text{Pb}$				$^{207}\text{Pb}/^{235}\text{U}$				$^{206}\text{Pb}/^{238}\text{U}$				$^{207}\text{Pb}/^{206}\text{Pb}$			
				1 σ	1 σ	1 σ	1 σ	1 σ	1 σ	1 σ	1 σ	1 σ	1 σ	1 σ	1 σ	1 σ	1 σ	1 σ	
CT-BC Medium-grained biotite Granite																			
CT-BC-01	974	2287	0.43	0.0552	0.0039	0.0282	0.0020	0.0037	0.0001	420.42	157.39	28.24	2.00	23.79	0.45				
CT-BC-02	4974	6849	0.73	0.0471	0.0017	0.0238	0.0008	0.0037	0.0000	57.50	81.48	23.84	0.78	23.57	0.27				
CT-BC-03	4347	6780	0.64	0.0530	0.0042	0.0279	0.0029	0.0037	0.0000	327.84	179.61	27.96	2.82	23.56	0.29				
CT-BC-04	4088	5271	0.78	0.0487	0.0018	0.0244	0.0008	0.0036	0.0000	200.08	80.55	24.50	0.80	23.45	0.26				
CT-BC-05	4007	8241	0.49	0.0463	0.0018	0.0238	0.0011	0.0037	0.0000	13.06	88.88	23.86	1.08	23.58	0.29				
CT-BC-06	4732	8396	0.56	0.0473	0.0015	0.0243	0.0007	0.0037	0.0000	64.91	77.77	24.38	0.74	23.87	0.25				
CT-BC-07	3416	4537	0.75	0.0509	0.0022	0.0260	0.0011	0.0037	0.0001	235.25	65.73	26.02	1.11	23.73	0.37				
CT-BC-08	5161	9752	0.53	0.0497	0.0018	0.0250	0.0009	0.0037	0.0000	188.97	82.40	25.02	0.85	23.57	0.32				
CT-BC-09	2889	4227	0.68	0.0567	0.0026	0.0284	0.0012	0.0037	0.0000	479.67	99.99	28.47	1.18	23.52	0.28				
CT-BC-10	6977	11,816	0.59	0.0583	0.0020	0.0298	0.0011	0.0037	0.0000	538.93	74.06	29.83	1.09	23.52	0.26				
CT-BC-11	5053	8559	0.59	0.0557	0.0023	0.0284	0.0012	0.0037	0.0001	442.64	90.73	28.47	1.16	23.62	0.34				
CT-BC-12	4899	9782	0.50	0.0482	0.0019	0.0246	0.0009	0.0037	0.0001	105.65	92.59	24.71	0.92	24.00	0.35				
CT-BC-13	3506	7717	0.45	0.0469	0.0017	0.0240	0.0009	0.0037	0.0000	42.69	88.88	24.05	0.93	23.74	0.28				
CT-BC-14	2974	5606	0.53	0.0481	0.0021	0.0246	0.0010	0.0037	0.0000	105.65	99.98	24.63	0.98	23.82	0.31				
CT-BC-15	2121	4176	0.51	0.0491	0.0024	0.0251	0.0011	0.0037	0.0000	153.79	112.95	25.16	1.06	23.90	0.30				
CT-BC-16	1470	2935	0.50	0.0645	0.0039	0.0340	0.0026	0.0037	0.0001	766.67	123.14	33.97	2.54	23.74	0.40				
CT-BC-17	1372	3697	0.37	0.0495	0.0032	0.0253	0.0015	0.0037	0.0001	172.31	154.61	25.39	1.51	23.99	0.35				
CT-BC-18	1195	2226	0.54	0.0490	0.0030	0.0250	0.0015	0.0037	0.0001	146.38	140.72	25.08	1.44	23.93	0.39				
CT-BC-19	11,053	14,341	0.77	0.0716	0.0049	0.0379	0.0029	0.0037	0.0000	975.93	140.74	37.77	2.86	23.72	0.28				
CT-BC-20	2216	3808	0.58	0.0553	0.0026	0.0286	0.0014	0.0037	0.0001	433.38	103.69	28.63	1.37	23.93	0.33				
CT-BC-21	2122	4786	0.44	0.0479	0.0026	0.0249	0.0013	0.0038	0.0001	100.09	116.65	24.95	1.31	24.23	0.35				
CT-BC-22	412	456	0.90	0.0520	0.0091	0.0261	0.0033	0.0038	0.0001	283.40	359.22	26.19	3.26	24.16	0.82				
CT-BC-23	2588	4307	0.60	0.0460	0.0019	0.0237	0.0009	0.0038	0.0000	57.50	81.48	23.80	0.91	24.25	0.25				
CT-BC-24	955	2638	0.36	0.0473	0.0024	0.0241	0.0012	0.0037	0.0000	64.91	124.06	24.14	1.15	23.98	0.28				
CT-BC-25	2893	3815	0.76	0.0483	0.0020	0.0252	0.0010	0.0038	0.0000	122.31	96.28	25.25	1.01	24.40	0.31				
CT-BC-26	2094	5187	0.40	0.0490	0.0019	0.0253	0.0010	0.0037	0.0000	150.09	88.88	25.37	0.97	24.00	0.25				
BN-BC3 Fine-grained biotite granite																			
BN-BC3-01	577	4395	0.13	0.0474	0.0026	0.0282	0.0019	0.0043	0.0001	77.87	116.66	28.24	1.89	27.38	0.81				
BN-BC3-02	723	829	0.87	0.0486	0.0070	0.0264	0.0035	0.0041	0.0001	131.57	307.37	26.48	3.43	26.51	0.56				
BN-BC3-03	954	1895	0.50	0.0512	0.0081	0.0256	0.0017	0.0041	0.0001	255.62	320.34	25.70	1.66	26.42	0.49				
BN-BC3-04	703	3253	0.22	0.0564	0.0027	0.0342	0.0018	0.0044	0.0001	477.82	102.77	34.10	1.76	28.32	0.76				
BN-BC3-05	366	369	0.99	0.0631	0.0097	0.0316	0.0029	0.0041	0.0002	722.23	333.31	31.62	2.87	26.54	1.01				
BN-BC3-06	575	665	0.87	0.0485	0.0042	0.0276	0.0019	0.0043	0.0001	124.16	192.56	27.61	1.87	27.58	0.63				
BN-BC3-07	1092	1078	1.01	0.0468	0.0053	0.0257	0.0021	0.0041	0.0001	42.69	257.37	25.79	2.11	26.27	0.64				
BN-BC3-08	464	389	1.12	0.0605	0.0107	0.0314	0.0052	0.0041	0.0001	620.39	389.62	31.43	5.11	26.67	0.84				
BN-BC3-09	388	305	1.27	0.0491	0.0076	0.0263	0.0039	0.0041	0.0001	153.79	325.88	26.32	3.89	26.64	0.90				
BN-BC3-10	231	201	1.15	0.0668	0.0118	0.0307	0.0031	0.0041	0.0002	831.48	375.90	30.72	3.05	26.12	1.13				
BN-BC3-11	179	192	0.93	0.0558	0.0093	0.0272	0.0025	0.0041	0.0002	455.60	377.73	27.26	2.52	26.46	1.00				
BN-BC3-12	547	1446	0.38	0.0470	0.0034	0.0262	0.0018	0.0041	0.0001	50.10	166.65	26.30	1.74	26.26	0.46				
BN-BC3-13	1041	1738	0.60	0.0485	0.0043	0.0269	0.0023	0.0042	0.0001	124.16	196.27	26.92	2.26	26.81	0.83				
BN-BC3-14	450	350	1.28	0.0499	0.0070	0.0272	0.0034	0.0040	0.0001	187.12	299.96	27.28	3.39	25.90	0.75				
BN-BC3-15	679	810	0.84	0.0482	0.0045	0.0275	0.0023	0.0042	0.0001	122.31	194.42	27.53	2.31	26.94	0.58				
BN-BC3-16	270	376	0.72	0.0556	0.0083	0.0281	0.0034	0.0041	0.0001	435.23	329.43	28.10	3.38	26.08	0.77				
BN-BC3-17	212	248	0.86	0.0580	0.0102	0.0252	0.0041	0.0040	0.0001	531.52	387.92	25.23	4.06	25.57	0.81				
BN-BC3-18	63.3	391	0.16	0.0507	0.0029	0.2678	0.0151	0.0381	0.0007	227.85	126.84	240.9	12.12	240.8	2.45				
BN-BC3-19	83.3	469	0.18	0.0542	0.0027	0.2878	0.0139	0.0387	0.0010	388.94	119.43	256.8	10.95	245.0	3.90				
BN-BC3-20	65.5	362	0.18	0.0562	0.0024	0.2985	0.0132	0.0385	0.0007	461.16	96.288	265.3	10.29	243.2	4.28				
BN-BC3-21	76.9	381	0.20	0.0518	0.0025	0.2764	0.0141	0.0381	0.0006	275.99	108.32	247.8	11.22	241.2	3.87				
BN-BC3-22	80.2	655	0.12	0.0600	0.0031	0.3160	0.0225	0.0378	0.0018	611.13	111.09	278.9	17.33	241.3	1.41				
BN-BC3-23	70.2	342	0.20	0.0536	0.0025	0.2910	0.0136	0.0391	0.0005	353.76	100.92	259.4	10.68	247.2	3.26				
BN-BC3-24	93.1	450	0.21	0.0526	0.0022	0.2749	0.0101	0.0380	0.0005	322.28	94.43	246.6	8.04	240.1	2.96				
BN-BC3-25	102	512	0.20	0.0543	0.0030	0.2842	0.0187	0.0387	0.0019	388.94	122.21	254.0	14.81	244.7	3.93				

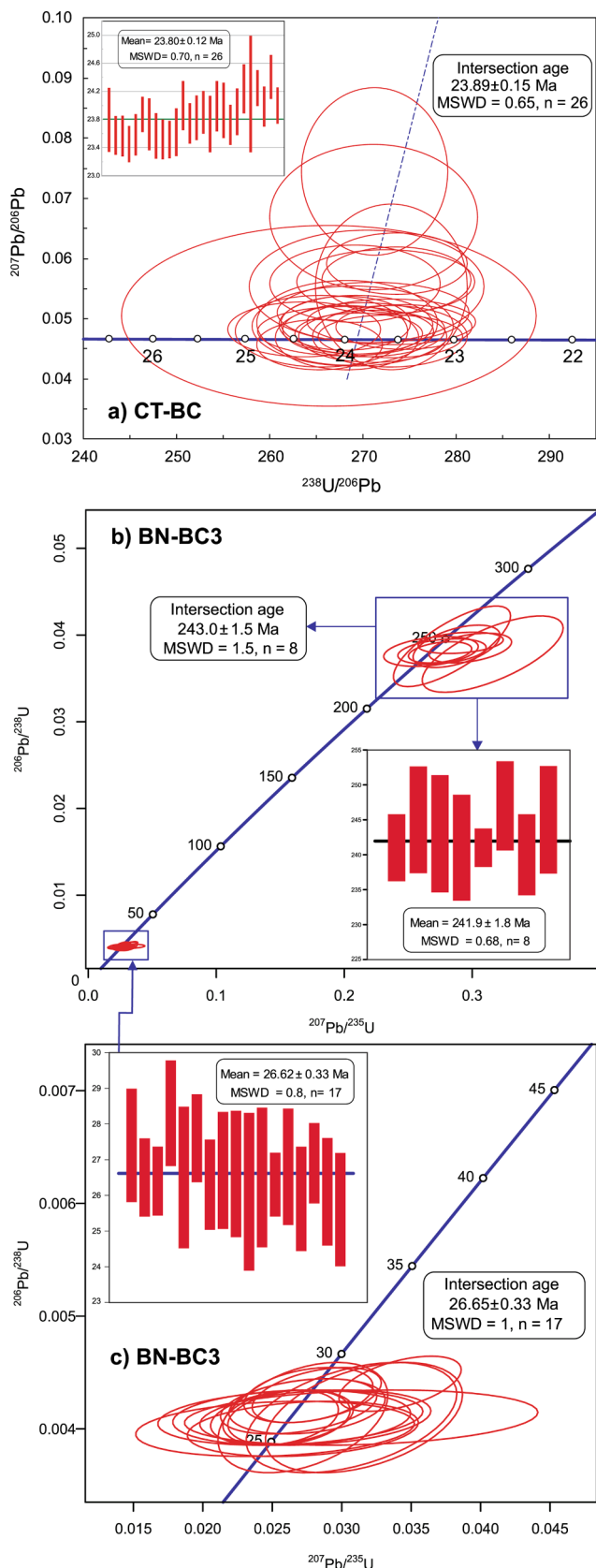


Fig. 8. The Tera-Wasserburg Concordia diagram, $^{206}\text{Pb}/^{238}\text{U}$ - $^{207}\text{Pb}/^{235}\text{U}$ Concordia diagram, and weighted mean age of zircon obtained from biotite granite in Quy Hop.

158.2 ± 0.4 Ma (Yuan et al., 2011). The internal texture of the cassiterites was characterised using scanning electron microscopy (SEM) and CL images.

Each set of six spot analyses was followed by three analyses of AY-4 (Yuan et al., 2011) and one analysis of NIST SRM 612 (Pearce et al., 1997; Kent et al., 2004; Kent, 2008; Jenner et al., 2009). The laser produced an ablation pit with a diameter of 50 μm at a pulse rate of 8 Hz and energy density of 4 J/cm² in the analysis of these cassiterite grains. Each analysis consisted of approximately 20 s of background acquisition, followed by 40 s of data acquisition, with a 50 s delay between analyses. During the U-Pb dating process, the dwell time of each mass scan was set to 25 ms for ^{238}U , ^{232}Th , ^{208}Pb , ^{206}Pb , ^{204}Pb , and ^{202}Hg and 40 ms for ^{207}Pb .

In situ U-Pb dating of cassiterite samples was performed using a Thermal iCAP Qc ICP-MS coupled with a Resonetics RESolution S-155 LA system at the State Key Laboratory of Geological Processes and Mineral Resources, China University of Geosciences, Wuhan. Raw data reduction was performed offline using the ICPMSDataCal 10.9 software (Liu et al., 2010; Lin et al., 2016). The uncorrected cassiterite composition measurements were plotted on a Tera-Wasserburg Concordia diagram (Tera and Wasserburg, 1972), in which the Concordia line intercepts the Y-axis at the common $^{207}\text{Pb}/^{206}\text{Pb}$ value; the Concordia line with a lower intercept value represents the sample formation age. The cassiterite U-Pb age calculation and Concordia diagrams were plotted online using the software IsoplotR (Vermeesch, 2018). Uncertainty was determined as 2σ .

4. Analytical results

4.1. Zircon U-Pb ages

Zircon grains from two granite samples selected for LA-ICP-MS U-Pb dating were mostly yellowish brown, colourless, transparent, with some grains containing black inclusions. Most zircon grains were prismatic with length/width ratios ranging from 3:1 to 2:1. Most zircons grains were 50–200 μm in length and 30–100 μm in width, with a euhedral shape and clear oscillatory zoning (Fig. 7). Zircon grains with clear zonation, without mineral inclusions and cracks, were chosen for U-Pb dating. The results of the zircon LA-ICP-MS analysis are presented in Table 1. Their Th/U ratios, ranging from 0.12 to 1.28, indicate that the zircons were formed primarily from magmatic solution (Belousova et al., 2002).

A total of 26 spots on 22 zircon grains from the medium-grained biotite granite sample CT-BC were analysed for U-Pb isotope compositions. The concentrations of Th (412–11,053 ppm) and U (456–14,341 ppm) and Th/U ratios (0.36–0.90, with an average of 0.58), indicate magmatic origin (Table 1; Fig. 7a). The resulting U-Pb data yielded an intersection and representative granite crystallisation age of 23.89 ± 0.15 Ma ($n = 26$, MSWD = 0.65), which was in accordance with the weighted mean $^{206}\text{Pb}/^{238}\text{U}$ age of 23.80 ± 0.12 Ma ($n = 26$, MSWD = 0.70) (Fig. 8a).

A total of 25 spots on 24 zircon grains obtained from the fine-grained biotite granite sample BN-BC3 were analysed. They comprised prismatic crystals with an oscillatory zoning structure and several black inclusions. The LA-ICP-MS U-Pb dating results of BN-BC3 exhibited two age groups (Table 1). Seventeen spots yielded $^{206}\text{Pb}/^{238}\text{U}$ ages of 28.32–25.57 Ma. The associated U and Th concentrations of the zircon grains were 192–4,395 ppm and 179–1,092 ppm, respectively, and the Th/U ratios ranged from 0.13 to 1.28, indicating the magmatic origin of the grains. The weighted mean $^{206}\text{Pb}/^{238}\text{U}$ age was calculated as 26.62 ± 0.33 Ma ($n = 17$, MSWD = 0.8) and the intersection age as 26.65 ± 0.33 Ma ($n = 17$, MSWD = 1) (Fig. 8b and c). The other eight inherited grains exhibited older $^{206}\text{Pb}/^{238}\text{U}$ ages of 247.2–240.1 Ma, a mean $^{206}\text{Pb}/^{238}\text{U}$ age of 241.9 ± 1.8 Ma ($n = 8$, MSWD = 0.68, 2σ), and intersection age of 243.0 ± 1.5 Ma ($n = 8$, MSWD = 1.5) (Fig. 8b). The older zircon grains exhibited U and Th concentrations of 342–655 ppm

Table 2⁴⁰Ar/³⁹Ar dating results for a muscovite sample from a greisen tin ore in Ban Ngoc.

Step	Laser output	³⁶ Ar _{air} (fA)	³⁷ Ar _{Ca} (fA)	³⁸ Ar _{Cl} (fA)	³⁹ Ar _K (fA)	⁴⁰ Ar* (fA)	Age ± 2σ Ma	⁴⁰ Ar* %	³⁹ Ar %	³⁹ Ar/ ⁴⁰ Ar	± 2σ	³⁶ Ar/ ⁴⁰ Ar	± 2σ
<i>BN-Gre, J = 0.00747724 ± 0.00002243</i>													
1	4.2%	5.76881	1.46133	0.00000	150.10466	282.15552	25.24 ± 1.90	14.07	0.42	0.07488	± 0.00023	0.00288 ± 0.00004	
2	5.0%	6.79312	5.16079	0.01206	943.11315	1717.53783	24.46 ± 0.36	45.83	2.66	0.25179	± 0.00077	0.00181 ± 0.00002	
3	5.8%	5.25169	3.54096	0.01888	1634.79626	2905.24238	23.87 ± 0.17	64.89	4.62	0.36547	± 0.00111	0.00117 ± 0.00001	
4	6.6%	8.94119	3.42803	0.01042	1753.37339	3119.86872	23.90 ± 0.26	53.85	4.95	0.30286	± 0.00092	0.00154 ± 0.00002	
5	7.2%	3.59659	1.73715	0.00000	1387.23046	2460.79278	23.83 ± 0.15	69.56	3.92	0.39247	± 0.00120	0.00102 ± 0.00001	
6	8.0%	3.12651	0.93471	0.03175	1513.65374	2684.21472	23.82 ± 0.13	74.13	4.28	0.41841	± 0.00127	0.00086 ± 0.00001	
7	9.0%	4.31786	2.69880	0.00644	1554.11088	2765.49931	23.90 ± 0.16	68.15	4.39	0.38329	± 0.00117	0.00106 ± 0.00001	
8	10.0%	3.13074	2.05701	0.02072	1424.81833	2534.34908	23.89 ± 0.14	72.99	4.02	0.41072	± 0.00126	0.00090 ± 0.00001	
9	11.5%	4.27799	0.00000	0.03879	1616.05875	2868.03323	23.84 ± 0.15	69.13	4.57	0.38986	± 0.00118	0.00103 ± 0.00001	
10	13.0%	4.19363	0.00000	0.02119	1526.01832	2704.77290	23.81 ± 0.15	68.30	4.31	0.38567	± 0.00117	0.00106 ± 0.00001	
11	15.0%	4.13609	0.00000	0.00000	1319.14844	2349.87626	23.93 ± 0.18	65.50	3.73	0.36799	± 0.00112	0.00115 ± 0.00002	
12	18.0%	3.13183	0.00000	0.06545	1439.23022	2555.08682	23.85 ± 0.13	73.14	4.07	0.41237	± 0.00125	0.00090 ± 0.00001	
13	21.0%	2.22605	0.00000	0.01161	1287.75435	2291.64010	23.90 ± 0.12	77.44	3.64	0.43560	± 0.00134	0.00075 ± 0.00001	
14	24.0%	2.29693	0.00000	0.00975	1226.17844	2178.49130	23.86 ± 0.12	75.98	3.46	0.42810	± 0.00130	0.00080 ± 0.00001	
15	27.0%	2.70186	0.74764	0.02730	1229.76825	2182.85448	23.84 ± 0.13	72.95	3.47	0.41136	± 0.00125	0.00090 ± 0.00001	
16	30.0%	4.34321	1.45236	0.03436	1797.49722	3204.71883	23.95 ± 0.14	71.13	5.08	0.39932	± 0.00122	0.00096 ± 0.00001	
17	34.0%	3.61550	2.45440	0.03243	2408.17665	4285.37647	23.90 ± 0.11	79.80	6.80	0.44888	± 0.00136	0.00067 ± 0.00001	
18	38.0%	4.34599	1.23342	0.04346	2449.71823	4360.69787	23.91 ± 0.11	76.99	6.92	0.43295	± 0.00132	0.00077 ± 0.00001	
19	42.0%	4.44584	1.76576	0.04999	2881.38210	5125.87652	23.90 ± 0.11	79.35	8.14	0.44650	± 0.00136	0.00069 ± 0.00001	
20	46.0%	1.76386	1.30019	0.09225	2074.98989	3690.75424	23.89 ± 0.09	87.41	5.86	0.49201	± 0.00149	0.00042 ± 0.00001	
21	50.0%	1.46675	0.00000	0.06088	1827.35126	3241.03243	23.82 ± 0.09	88.00	5.16	0.49671	± 0.00151	0.00040 ± 0.00001	
22	55.0%	1.08490	2.15155	0.02485	1054.30454	1869.48621	23.82 ± 0.10	85.14	2.98	0.48067	± 0.00145	0.00049 ± 0.00001	
23	60.0%	1.58223	1.40752	0.02227	901.47995	1604.50898	23.91 ± 0.13	77.18	2.55	0.43405	± 0.00131	0.00076 ± 0.00001	

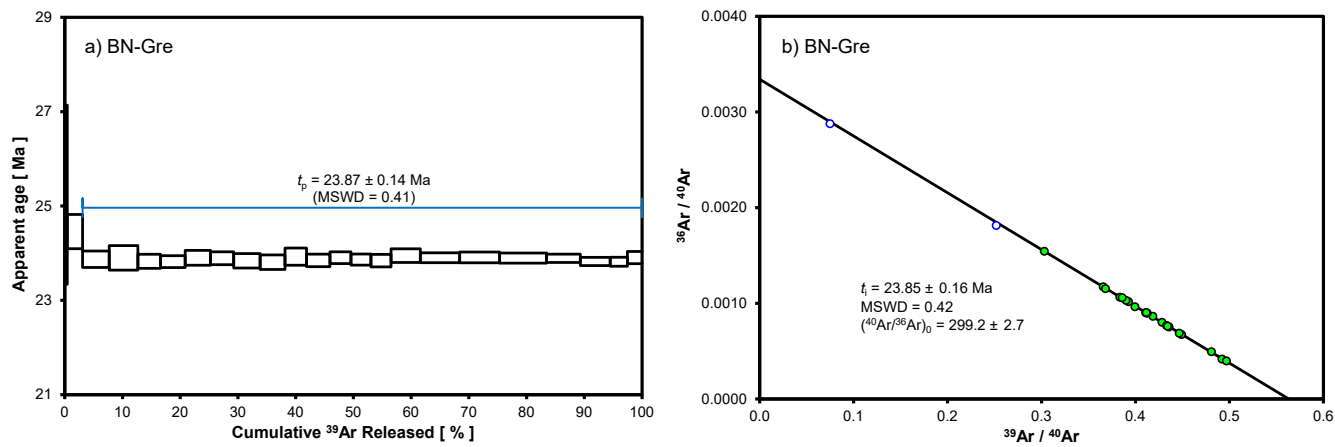
**Fig. 9.** (a) ⁴⁰Ar/³⁹Ar plateau age spectra and (b) inverse isochron of muscovite in sample BN-Gre collected at Ban Ngoc.

Table 3

LA-ICP-MS U-Pb dating results for cassiterite samples from tin ores.

Sample spots	Isotopic ratios and errors ($\pm 2\sigma$)						Ages (Ma) and errors ($\pm 2\sigma$)	
	$^{207}\text{Pb}/^{206}\text{Pb}$	2σ	$^{238}\text{U}/^{206}\text{Pb}$	2σ	$^{207}\text{Pb}/^{235}\text{U}$	2σ	$^{206}\text{Pb}/^{238}\text{U}$	2σ
Quartz-type ore (SB-1)								
1	0.82056	0.05202	4.95254	0.33392	22.84459	1.74811	27.7	1.9
2	0.55464	0.03402	85.83524	4.08611	0.89093	0.05221	26.8	1.3
3	0.70982	0.03585	35.93847	1.51171	2.72325	0.12980	28.9	1.2
4	0.54606	0.04320	82.57138	6.32912	0.91182	0.08365	28.7	2.2
5	0.43337	0.04136	110.80266	8.16529	0.53928	0.05267	29.7	2.2
6	0.40765	0.04687	141.47403	8.32933	0.39729	0.03940	24.7	1.5
7	0.67513	0.04075	59.24189	4.53389	1.57129	0.13109	23.3	1.7
8	0.75016	0.04511	28.07570	2.29829	3.68404	0.32514	25.3	2.1
9	0.76898	0.04677	24.48863	1.65566	4.32961	0.32702	22.8	1.5
10	0.71109	0.03025	33.73483	1.66670	2.90636	0.14636	30.5	1.5
11	0.66183	0.02894	58.51390	4.95775	1.55950	0.19920	25.8	1.2
12	0.64722	0.03889	52.41238	3.27029	1.70263	0.12014	29.5	1.8
13	0.75198	0.04722	29.63401	1.54713	3.49878	0.21982	26.6	1.4
14	0.44241	0.04099	119.04188	2.27156	0.51241	0.13317	27.4	1.2
15	0.77012	0.05789	26.15689	1.79222	4.05949	0.33813	24.6	1.7
16	0.70903	0.11195	95.68168	6.79896	1.02173	0.13653	10.9	0.8
17	0.11364	0.04247	174.04244	10.76463	0.09003	0.02542	44.39	2.8
Greisen-type ore (BN-Gre)								
1	0.45848	0.02801	98.30127	13.53133	0.17164	0.10432	26.8	3.5
2	0.71675	0.08997	22.09137	2.55124	4.47352	0.66735	25.1	3.6
3	0.78340	0.03433	11.21154	0.47584	9.63433	0.44127	28.5	1.3
4	0.11765	0.03304	259.04387	13.22559	0.06029	0.01367	21.7	1.2
5	0.51124	0.03825	93.94127	6.65571	0.75037	0.06545	27.5	3.0
6	0.07498	0.01290	261.15664	11.45865	0.03677	0.00514	22.1	1.0
7	0.19439	0.02784	219.93882	15.30504	0.12186	0.01576	23.7	1.6
8	0.08854	0.01495	264.90965	12.4943	0.04609	0.00637	23.0	1.1
9	0.76711	0.06264	26.76436	1.88764	3.95188	0.35860	22.6	1.2
10	0.29964	0.03412	186.11685	10.51419	0.22198	0.02261	23.3	1.3
11	0.89409	0.09509	31.59803	2.28003	3.90143	0.41582	24.0	1.0
12	0.76711	0.06264	26.76436	1.88764	3.95188	0.35860	22.6	1.2
13	0.89109	0.09609	30.99803	2.28003	3.90143	0.41582	22.3	1.0
14	0.37644	0.06471	188.98381	14.74242	0.27465	0.04223	23.6	1.5
15	0.91582	0.13631	32.41312	2.20157	3.89577	0.51610	24.0	2.0
16	0.60420	0.03322	74.72933	5.90508	1.11479	0.09477	24.3	1.9
17	0.36999	0.03512	169.64033	8.71911	0.30072	0.02577	22.2	1.1
18	0.50783	0.04152	127.4209	6.96025	0.54952	0.04337	22.0	1.1
19	0.16612	0.02726	231.5392	11.67489	0.09892	0.01335	23.5	1.2
20	0.37544	0.06471	188.98381	14.73942	0.27465	0.04223	21.6	1.4
21	0.70116	0.05936	30.68161	4.10659	3.15098	0.46099	26.1	3.4
22	0.25174	0.02914	204.49799	12.35887	0.16973	0.01784	23.2	1.4
23	0.21991	0.05487	220.33921	15.17166	0.13761	0.03111	22.7	2.6
24	0.07623	0.01332	259.53286	13.98617	0.03747	0.00554	22.1	1.2
25	0.53367	0.05212	18.93556	2.09484	3.88588	0.51247	125.9	13.9

and 63.3–102 ppm, respectively, with Th/U ratios of 0.12–0.21, indicating that they were formed from magmatic solution. Based on these dating results, the crystallization age of the fine-grained biotite granite was determined to be 26.65 ± 0.33 Ma.

4.2. Muscovite $^{40}\text{Ar}/^{39}\text{Ar}$ ages

The $^{40}\text{Ar}/^{39}\text{Ar}$ dating results obtained for muscovite in sample BN-Gre via stepwise laser heating are presented in Table 2. The plots of the age spectrum and inverse isochron are shown in Fig. 9. The $^{40}\text{Ar}/^{39}\text{Ar}$ muscovite ages exhibited minimal deviation, with a plateau of 23.87 ± 0.14 Ma (2σ , MSWD = 0.41, $\sum^{39}\text{Ar} = 97\%$), except for those calculated at the first two steps (Fig. 9a). The data points constituting the plateau represent an isochron line corresponding to an age of 23.85 ± 0.16 Ma (MSWD = 0.42) (Fig. 9b), with an initial ($^{40}\text{Ar}/^{36}\text{Ar}_0$) ratio of 299.2, which is very close to the modern atmospheric ration of 298.56 (Lee et al., 2006). The close relationship between the plateau and isochron ages strongly supports a tin mineralisation age of 23.9 Ma for Ban Ngoc.

4.3. Cassiterite U-Pb ages

The cassiterite grains obtained from the two samples were yellow to

dark brown in colour and contained minor cracks (Fig. 6). Cathodoluminescence images showed that most cassiterite grains were euhedral to subhedral in shape, 40–700 μm long, 40–450 μm wide, and mostly without zoning in back-scattered electron (BSE) images. The largest cassiterite grains, with an average length of 400 μm and width of 300 μm and short, prismatic shape, were obtained from the hydrothermal quartz veins of sample SB-1 (Fig. 6a and c). In contrast, grains obtained from the greisen of sample BN-Gre were much smaller (Fig. 6b and d). Furthermore, some cassiterite grains from both samples were highly luminescent, while others were dark.

The cassiterite spots analysed by LA-ICP-MS U-Pb dating were selected to avoid inclusions and cracks. The results for SB-1 and BN-Gre are listed in Table 3 and associated Tera-Wasserburg Concordia diagrams ($^{207}\text{Pb}/^{206}\text{Pb}$ versus $^{238}\text{U}/^{206}\text{Pb}$) are plotted in Fig. 10. Seventeen cassiterite spots from sample SB-1 were analysed (Fig. 6a). The ratios of $^{238}\text{U}/^{206}\text{Pb}$ and $^{207}\text{Pb}/^{206}\text{Pb}$ were 4.95254–119.04188 and 0.40765–0.82056, respectively (Table 3). The analyses yielded a reliable intersection age of 26.81 ± 1.92 Ma ($n = 15$, MSWD = 0.87, 2σ) (Fig. 10a). Twenty-five cassiterite spots from sample BN-Gre were analysed (Fig. 6c). These spots exhibited $^{238}\text{U}/^{206}\text{Pb}$ ratios of 11.21154–264.90965 and $^{207}\text{Pb}/^{206}\text{Pb}$ ratios of 0.07498–0.91582 (Table 3), yielding an intersection and representative tin mineralisation age of 23.23 ± 0.89 Ma ($n = 24$, MSWD = 2.9, 2σ) on Tera-Wasserburg

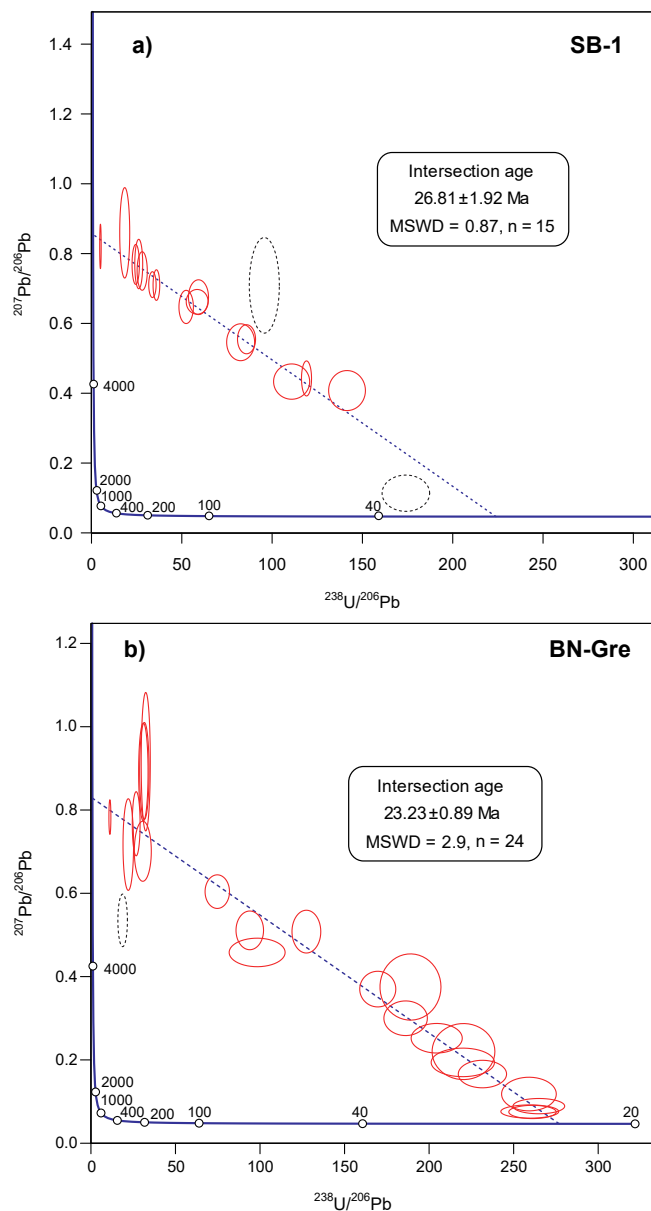


Fig. 10. $^{238}\text{U}/^{206}\text{Pb}$ - $^{207}\text{Pb}/^{206}\text{Pb}$ isochron diagram of cassiterite obtained from (a) Suoi Bac and (b) Ban Ngoc.

Concordia diagram (Fig. 10b). Based on the intersection ages obtained for quartz ore from Suoi Bac in sample SB-1 and greisen ore from Ban Ngoc in sample BN-Gre, tin mineralisation in Quy Hop can be dated at 23–26 Ma.

5. Discussion

5.1. Emplacement ages of Ban Chieng granitic rocks

Magmatic rocks of the Ban Chieng Complex in the Phu Hoat Terrane have been dated to the Palaeogene period in previous studies (Table 4) (Lepvrier et al., 1997; Jolivet et al., 1999; Nagy et al., 2000; Garnier et al., 2002; Trung et al., 2007; Nguyen et al., 2014; Bui et al., 2017; Trinh et al., 2021). The results reported in these studies cover a relatively wide age range from 29.5 to 22.1 Ma. Trung et al. (2007) reported whole-rock Rb-Sr isochron ages of 27 ± 1 Ma and biotite K-Ar ages of 24.7–24.2 Ma for the porphyritic alkali feldspar granite. Biotite $^{40}\text{Ar}/^{39}\text{Ar}$ ages of 27.3–22.1 Ma were obtained for granitic pegmatite

and biotite granite (Lepvrier et al., 1997; Jolivet et al., 1999; Garnier et al., 2002). In the Bu Khang Dome, zircon and monazite U-Pb dating yielded ages of 26.0–23.7 Ma for granitoid intrusions (Nagy et al., 2000), and zircon LA-ICP-MS dating of biotite granite, porphyritic granite, and granosyenite yielded U-Pb ages of 28.62–24.70 Ma (Trinh et al., 2021). Lastly, zircon SHRIMP U-Pb ages of 29.5–27.4 Ma were reported for the granitic rocks of the Ban Chieng Complex (Bui et al., 2017).

To identify the exact magmatic source rocks of the tin mineralisation at Quy Hop, the intrusion ages of the various granite phases within the Ban Chieng Complex should be studied in greater detail using modern isotopic dating techniques. In this study, using zircon LA-ICP-MS U-Pb dating, the ages of biotite granite in Ban Ngoc and Chau Tien were determined to be 26.65 ± 0.33 Ma and 23.89 ± 0.15 Ma, respectively (Fig. 8). The new age data are consistent with previous $^{40}\text{Ar}/^{39}\text{Ar}$, U-Pb, and Rb-Sr ages and confirm that the emplacement of granitic rocks in the Ban Chieng Complex of the Phu Hoat Terrane occurred in the Late Oligocene (Fig. 11, Table 4).

5.2. Age of tin mineralisation at Quy Hop

Because of its high K content and high retention capacity for radiogenic Ar, muscovite is one of the minerals best suited for use in $^{40}\text{Ar}/^{39}\text{Ar}$ dating with previous studies (Bai et al., 2018a; Bai et al., 2019; Xiao et al., 2019) confirming its ability to yield precise tin-tungsten mineralisation ages. Direct dating of cassiterite ore using the LA-ICP-MS U-Pb method has also served as a robust geochronometer for dating tin mineralisation events (Chen et al., 2014; Cao et al., 2017; Chen et al., 2018; Zhang et al., 2019a; Zhang et al., 2020; Moscati and Neymark, 2020). For many years, tin deposits at Quy Hop have been studied in terms of their mineralogical characteristics and chemical composition, but not mineralisation ages.

The muscovite $^{40}\text{Ar}/^{39}\text{Ar}$ ages obtained in this study from greisen ore in Ban Ngoc (sample BN-Gre) exhibited little variation, with a high-precision plateau age of 23.87 ± 0.14 Ma in accordance with an isochron age of 23.85 ± 0.16 Ma and an initial $(^{40}\text{Ar}/^{36}\text{Ar})_0$ ratio of 299.2 ± 2.7 in accordance with the modern atmospheric ratio of 298.56 (Lee et al., 2006). These values represent the muscovite crystallisation age, rather than cooling age, because the homogenisation temperature range of ore-forming fluid inclusions in quartz veins of 220–400 °C (Sao, 2008) is lower than the muscovite closure temperature of 425 °C (Harrison et al., 2009). When dated using the LA-ICP-MS U-Pb method, cassiterite grains from sample BN-Gre yielded an intersection age of 23.23 ± 0.89 Ma, in accordance with the muscovite $^{40}\text{Ar}/^{39}\text{Ar}$ age. The LA-ICP-MS U-Pb dating method also yielded an intersection age of 26.81 ± 1.92 Ma, for cassiterite grains from quartz vein ore in Suoi Bac (sample SB-1). Based on the muscovite $^{40}\text{Ar}/^{39}\text{Ar}$ and cassiterite U-Pb ages obtained in this study, tin mineralisation at Quy Hop likely occurred in the Late Oligocene (ca. 26–23 Ma).

5.3. Genetic relationship between Ban Chieng granitic intrusions and tin mineralisation

Most tin deposits are closely related to granitic intrusions in both space and time (Hosking, 1977; Taylor, 1979; Hutchison, 1984; Heinrich and Eadington, 1986), and biotite granite is particularly associated with tin mineralisation (Olade, 1980; Zhang et al., 2015; Zhang et al., 2017b). Compared to other tin-related granites, Duong et al. (1983) proposed that the age of the granitic Ban Chieng Complex is especially closely linked with that of tin mineralisation at Quy Hop.

Zircon LA-ICP-MS U-Pb dating results indicate that biotite granite was emplaced at 26.65 Ma and 23.89 Ma in the Ban Ngoc and Chau Tien outcrops of the Ban Chieng Complex, respectively. Muscovite $^{40}\text{Ar}/^{39}\text{Ar}$ and cassiterite LA-ICP-MS U-Pb ages suggest that tin deposits in Quy Hop date to 26–23 Ma. The significant overlap between granitoid and ore formation ages suggests that biotite granite emplacement might

Table 4

Summary of geochronological ages of igneous rocks from the Ban Chieng Complex.

No.	Sample name	Rock type	Mineral analyzed	Dating method	Result (Ma)	References
1	FL13	Granite	Biotite	K-Ar	24.5 ± 0.6	(Trung et al., 2007)
2	MC-12	Pegmatite	Biotite	Ar-Ar	22.5 ± 0.5	(Garnier et al., 2002)
3	VN230	Pegmatite	Biotite	Ar-Ar	22.1 ± 1.3	(Leprvier et al., 1997)
4	VN9717	Granite	Biotite	Ar-Ar	27.3 ± 0.5	(Jolivet et al., 1999)
5	VN9705	Granite	Biotite	Ar-Ar	26.4 ± 1.1	(Jolivet et al., 1999)
6	BCG	Porphyritic granite	Biotite	Rb-Sr	27 ± 1	(Trung et al., 2007)
7	VGS-32	Granite	Monazite	U-Pb	26.0 ± 0.2	(Nagy et al., 2000)
8	VGS-33	Granite	Monazite	U-Pb	23.7 ± 1.6	(Nagy et al., 2000)
9	TL-137	Granosyenite	Zircon	SHRIMP U-Pb	29.5 ± 0.4	(Bui et al., 2017)
10	TL-234	Porphyritic granite	Zircon	SHRIMP U-Pb	27.2	(Bui et al., 2017)
11	TL-135	Porphyritic granite	Zircon	SHRIMP U-Pb	27.5 ± 0.6	(Bui et al., 2017)
12	BK-105	Biotite granite	Zircon	SHRIMP U-Pb	27.36 ± 0.36	(Nguyen et al., 2014)
13	TL156	Biotite granite	Zircon	SHRIMP U-Pb	27.47 ± 0.5	(Nguyen et al., 2014)
14	L-019	Porphyritic granite	Zircon	LA-ICP-MS U-Pb	24.70 ± 0.18	(Trinh et al., 2021)
15	L-030	Porphyritic granite	Zircon	LA-ICP-MS U-Pb	28.35 ± 0.28	(Trinh et al., 2021)
16	H-VN-012	Alskite granite	Zircon	LA-ICP-MS U-Pb	28.62 ± 0.89	(Trinh et al., 2021)
17	H-VN-002	Granosyenite	Zircon	LA-ICP-MS U-Pb	28.17 ± 0.52	(Trinh et al., 2021)
18	BN-BC3	Fine-grained biotite granite	Zircon	LA-ICP-MS U-Pb	26.65 ± 0.33	this study
19	GT-BC	Medium-grained Biotite Granite	Zircon	LA-ICP-MS U-Pb	23.89 ± 0.15	this study

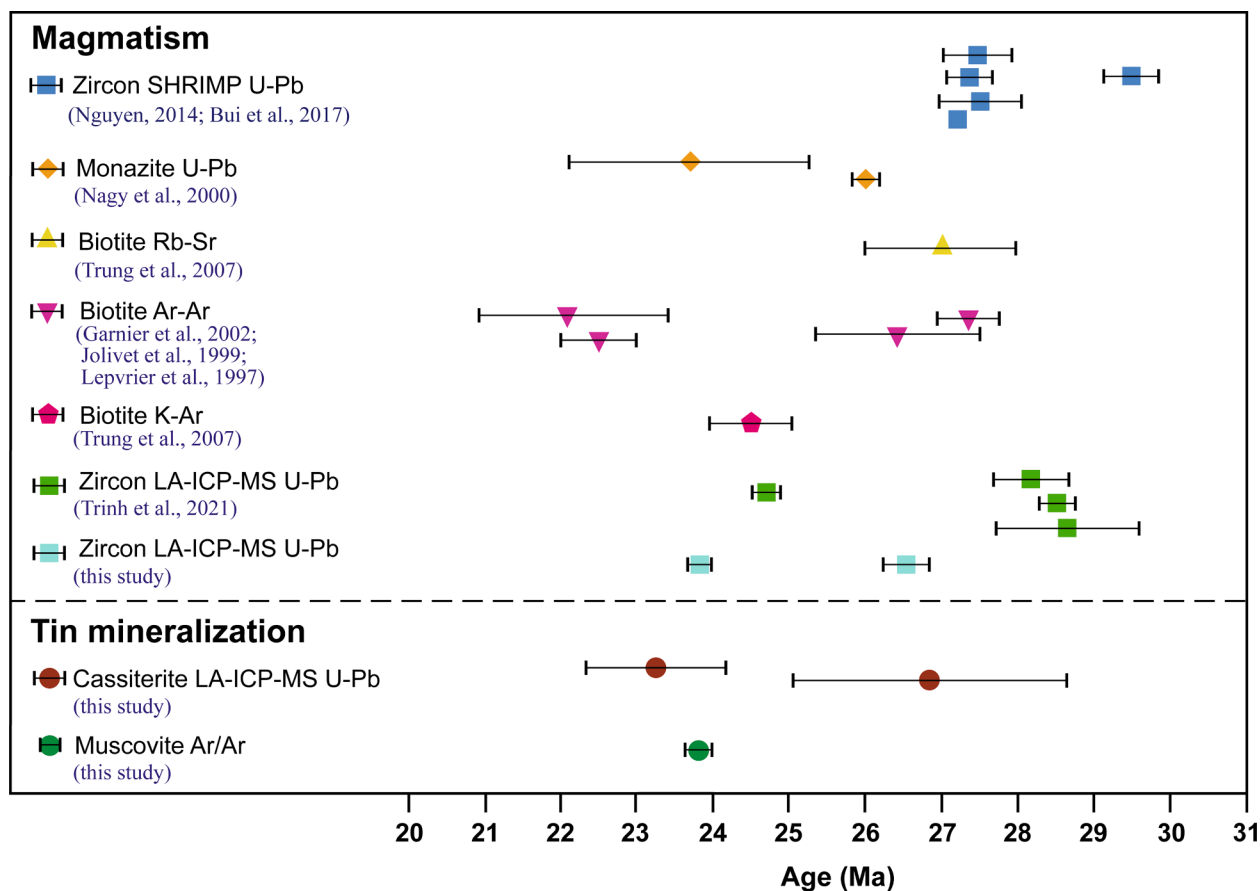


Fig. 11. Age range of granite samples obtained from the Ban Chieng Complex in the Phu Hoat Terrane (data sourced from Table 4).

have led to tin mineralisation in the Late Oligocene. Thus, the late Oligocene biotite granite of the Ban Chieng Complex in the Phu Hoat Terrane share a close spatial and temporal relationship with the quartz vein and greisen tin ore bodies in the area.

5.4. Tectonic and metallogenetic implications for the Phu Hoat Terrane

The ASRR is a major NW-SE strike-slip shear zone that separates the SW China and Indochina Terranes (Tapponnier et al., 1990; Leloup et al., 1995; Lacassin et al., 1997; Jolivet et al., 1999; Morley, 2002;

Wysocka and Świerczewska, 2010). The magmatic rocks in the zone including quartz-monzosyenite, two-mica granite, porphyritic granite, biotite granite, leucogranites, and granitic pegmatite, were directly related to the strike-slip movements in Late Oligocene, as shown in Fig. 1a (Schärer et al., 1990; Schärer et al., 1994; Zhang and Schärer, 1999; Liu et al., 2012b; He et al., 2019).

The Phu Hoat Terrane is located approximately 200 km south of the ASRR fault (Jolivet et al., 1999; Nagy et al., 2000). The biotite granite ages of 26.7–23.9 Ma (Fig. 8) coincide with the Late Oligocene – Early Miocene NW-SE extension of the Bu Khang Dome (36–21 Ma) (Leprvier

et al., 1997; Jolivet et al., 1999) as well as magmatic intrusions along the ASRR shear zone. In addition to tin mineralisation, other kinds of ore deposits in the Phu Hoat Terrane have also been linked to granitic intrusions in the Ban Chieng Complex. Garnier et al. (2002) found that ruby mineralisation in marbles and along pegmatite veins are linked to fine-grained biotite granite in the Quy Chau shear zone. Rare earth elements in weathered fine-grained biotite granite are exposed in the Chau Binh (Quy Chau), Tri Le (Que Phong), and Quy Hop districts (Heo et al., 2012; Heo et al., 2014; Lee et al., 2018). Nguyen et al. (2014) suggested that Sn-polymetallic skarn ore mineralisation in the Tri Le (Que Phong) region of the Phu Hoat Terrane (Fig. 1b) might be related to porphyritic granite and biotite granite in Ban Chieng, with zircon U-Pb ages of 29.5–27.2 Ma (Bui et al., 2017; Trinh et al., 2021).

The formation of the NW-SE extension of the Phu Hoat Terrane in northern Laos in Oligocene coincided with that of A- and S-type granites (28–24 Ma) in the Indochina Block (Fig. 1a, b). Their chemical and mineral compositions and emplacement ages are similar to those of Ban Chieng biotite granites (Wang et al., 2019; Trinh et al., 2021). It has been found that W-Sn-polymetallic ore mineralisation in Huoi Chun in north-eastern Laos might also be related to these intrusive rocks (Fig. 1a, b) (Luu et al., 2020; Trinh et al., 2021). Furthermore, it is highly possible that the Late Oligocene – Early Miocene granites associated with the ASRR left-lateral strike-slip movements resulted in mineralization in northern Vietnam and northern Laos, while the W-Sn deposits in Piaoao in northern Vietnam (Nguyen et al., 2019) and Gejiu-Dulong in southern Yunnan (Xu et al., 2015), both of which are north of the ASRR shear zone (Nguyen et al., 2019), were formed in the Late Cretaceous.

6. Conclusions

The main findings of this study can be summarised as follows:

- 1) LA-ICP-MS U-Pb dating of magmatic zircon indicates that biotite granite of the Ban Chieng Complex was emplaced at 26.7–23.9 Ma.
- 2) High-precision muscovite $^{40}\text{Ar}/^{39}\text{Ar}$ and novel cassiterite LA-ICP-MS U-Pb dating of greisen and quartz vein ores showed that tin mineralisation in Quy Hop occurred at 26.8–23.2 Ma.
- 3) The ages of tin mineralisation at Quy Hop strongly overlap with the emplacement ages of the Ban Chieng granite, suggesting tin mineralisation occurred during the waning stage of igneous activity in the Late Oligocene.
- 4) Many of the Late Oligocene granites that were emplaced during the left-lateral strike-slip event along the ASRR shear zone in northern Vietnam and northern Laos, respectively, could potentially be mineralised because W-Sn-polymetallic deposits were also found around the Late Oligocene granites (28–24 Ma) at Huoi Chun, northeast Laos, which have similar chemical and mineral compositions and emplacement ages to the Ban Chieng biotite granites.

Declaration of Competing Interest

The authors declare that they have no known competing financial interests or personal relationships that could have appeared to influence the work reported in this paper.

Acknowledgements

We are grateful to Franco Pirajno, Oliver Kreuzer, Rongqing Zhang, and an anonymous reviewer for their constructive suggestions and Shunda Yuan for his helpful input, which greatly improved the quality of the final manuscript. We also thank Duan Zhuang, Bin Tang, and Xiao Liu for their assistance with cassiterite LA-ICP-MS U-Pb dating and neutron irradiation, Nguyen Van Suong of Ha An Stannum Co., Ltd. for his guidance during fieldwork, and Dr. Guanzhong Shi for his feedback. This study was funded by the National Natural Science Foundation of China (grant number 41630315, 41873017, and 41688103) and the

Ministry of Education Plan 111 (grant number B20045).

References

- Bach, L.D., 1969. 1:200,000 Geological and Mineral Map of Quy Chau area. Geological Division of 20D. Publishing House of Sciences and Technology, Hanoi (in Vietnamese), p. 121.
- Bach, L.D., Quan, D.T., Mong, D.M., Kham, L.D.K., Minh, N.N., Minh, N.V., Nhan, N.T., Chu, N.T., Sang, N.V., Hung, P., Cu, P.N., Thanh, T.P.T., Bao, T.V., 2001. Geology and Mineral Resources Map of Vietnam Scale 1:200,000, Thanhhoa Sheet (E-48-IV). Department of Geology and Minerals of Vietnam, Hanoi (in Vietnamese), p. 126.
- Bai, X.J., Hu, R.G., Jiang, Y.D., Liu, X., Tang, B., Qiu, H.N., 2019. Refined insight into $^{40}\text{Ar}/^{39}\text{Ar}$ progressive crushing technique from K-Cl-Ar correlations in fluid inclusions. *Chem. Geol.* 515, 37–49.
- Bai, X.-J., Jiang, Y.-D., Hu, R.-G., Gu, X.-P., Qiu, H.-N., 2018a. Revealing mineralization and subsequent hydrothermal events: Insights from $^{40}\text{Ar}/^{39}\text{Ar}$ isochron and novel gas mixing lines of hydrothermal quartzes by progressive crushing. *Chem. Geol.* 483, 332–341.
- Bai, X.-J., Qiu, H.-N., Liu, W.-G., Mei, L.-F., 2018b. Automatic $^{40}\text{Ar}/^{39}\text{Ar}$ dating techniques using multicollector ARGUS VI noble gas mass spectrometer with self-made peripheral apparatus. *J. Earth Sci.* 29 (2), 408–415.
- Bai, X.J., Wang, M., Jiang, Y.D., Qiu, H.N., 2013. Direct dating of tin-tungsten mineralization of the Piaotang tungsten deposit, South China, by $^{40}\text{Ar}/^{39}\text{Ar}$ progressive crushing. *Geochim. Cosmochim. Acta* 114, 1–12.
- Belousova, E., Griffin, W., O'Reilly, S.Y., Fisher, N., 2002. Igneous zircon: trace element composition as an indicator of source rock type. *Contrib. Mineral. Petrol.* 143 (5), 602–622.
- Bracciali, L., Parrish, R.R., Horstwood, M.S.A., Condon, D.J., Najman, Y., 2013. U-Pb LA-(MC)-ICP-MS dating of rutile: New reference materials and applications to sedimentary provenance. *Chem. Geol.* 347, 82–101.
- Bui, D.C., Nguyen, T.B.T., Nguyen, C.D., Ta, D.T., 2017. SHRIMP zircon U-Pb isotope age of Ban Chieng granitoid in Phu Hoat structural zone and its geological implication. *J. Geol.*, Series B(46), 14–22.
- Cao, H.W., Zhang, Y.H., Pei, Q.M., Zhang, R.Q., Tang, L.i., Lin, B., Cai, G.J., 2017. U-Pb dating of zircon and cassiterite from the Early Cretaceous Jiaojiguan iron-tin polymetallic deposit, implications for magmatism and metallogeny of the Tengchong area, western Yunnan, China. *Int. Geol. Rev.* 59 (2), 234–258.
- Cao, S., Liu, J., Leiss, B., Neubauer, F., Genser, J., Zhao, C., 2011. Oligo-Miocene shearing along the Ailao Shan-Red River shear zone: constraints from structural analysis and zircon U/Pb geochronology of magmatic rocks in the Diancang Shan massif, SE Tibet, China. *Gondwana Res.* 19 (4), 975–993.
- Chen, L., Wang, Z., Yan, Z., Gong, J., Ma, S., 2018. Zircon and cassiterite U-Pb ages, petrogeochemistry and metallogenesis of Sn deposits in the Sibao area, northern Guangxi: constraints on the neoproterozoic granitic magmatism and related Sn mineralization in the western Jiangnan Orogen, South China. *Miner. Petrol.* 112 (4), 437–463.
- Carter, A., Roques, D., Bristow, C., Kinny, P., 2001. Understanding Mesozoic accretion in Southeast Asia: significance of Triassic thermotectonism (Indosinian orogeny) in Vietnam. *Geology* 29 (3), 211.
- Chen, X.C., Hu, R.Z., Bi, X.W., Li, H.M., Lan, J.B., Zhao, C.H., Zhu, J.J., 2014. Cassiterite LA-MC-ICP-MS U/Pb and muscovite $^{40}\text{Ar}/^{39}\text{Ar}$ dating of tin deposits in the Tengchong-Lianghe tin district, NW Yunnan, China. *Mineral. Deposita* 49 (7), 843–860.
- Chen, X.Y., Liu, J.L., Qi, Y.C., Fan, W.K., Ling, C.Y., 2017. Deformation characteristics of the granitic rocks from the mid-crustal shear zone and constraints on the tectono-magmatic relationship: exemplified by the Diancang Shan complex, western Yunnan. *Acta Petrol. Sin.* 33, 2241–2255.
- Deng, J., Wang, Q., Li, G., Zhao, Y., 2015. Structural control and genesis of the Oligocene Zhenyuan orogenic gold deposit, SW China. *Ore Geol. Rev.* 65, 42–54.
- Dovjikov, A., Bao, N.X., Van Chien, N., Luong, T.D., Van Quang, P., Izok, E., Marisev, A., Long, P.D., Zamoida, A., Ivanov, G., 1965. Geology of Northern Vietnam, Technical and Scientific Publisher, Hanoi (in Vietnamese), pp. 583.
- Duong, D.K., Shachnovsky, M.L., Le, V.T., Nguyen, V.N., Nguyen, T.K.H., Thai, Q.L., Nguyen, N.L., Do, H.D., Pham, V.L., 1983. Tin metallogeny of Vietnam. *J. Geol.* (in Vietnamese) 162, 12–16.
- Duong, V.H., Phan, T.T., Nguyen, T.D., Piestrzynski, A., Nguyen, D.C., Pieczonka, J., Ngo, X.D., Tran, V.P., Pham, T.B., Nguyen, V.H., Ngo, V.L., Bui, T.D., Vu, K.D., Bui, C.T., 2021. Cu-Au mineralization of the Sin Quyen deposit in north Vietnam: A product of Cenozoic left-lateral movement along the Red River shear zone. *Ore Geol. Rev.* 132, 104065.
- Elhou, S., Belousova, E., Griffin, W.L., Pearson, N.J., O'Reilly, S.Y., 2006. Trace element and isotopic composition of GJ-red zircon standard by laser ablation. *Geochim. Cosmochim. Acta* 70 (18), A158.
- Fromaget, J., 1941. L'Indochine Francaise, sa structure geologique, ses roches, ses mines et leur relation possible avec la tectonique. *Bull. Serv. Geol. Indoch.* 26, 140 pp.
- Garnier, V., Giuliani, G., Maluski, H., Ohnenstetter, D., Phan, T.T., Hoang, Q.V., Pham, V. L., Vu, V.T., Schwarz, D., 2002. Ar-Ar ages in phlogopites from marble-hosted ruby deposits in northern Vietnam: evidence for Cenozoic ruby formation. *Chem. Geol.* 188 (1–2), 33–49.
- Gulson, B.L., Jones, M.T., 1992. Cassiterite: Potential for direct dating of mineral deposits and a precise age for the Bushveld Complex granites. *Geology* 20 (4), 355.
- Harrison, T.M., Célérier, J., Aikman, A.B., Hermann, J., Heizler, M.T., 2009. Diffusion of ^{40}Ar in muscovite. *Geochim. Cosmochim. Acta* 73 (4), 1039–1051.

- He, X., Tan, S., Zhou, J., Liu, Z., Caulfield, J., Yang, S., Tian, H., 2019. Petrogenesis and tectonic implications of late Oligocene highly fractionated leucogranites in the Ailaoshan-Red River shear zone, SW China. *J. Asian Earth Sci.* 182, 103925.
- He, X., Tan, S., Zhou, J., Liu, Z., Zhao, Z., Yang, S., Zhang, Y., 2020. Identifying the leucogranites in the Ailaoshan-Red River shear zone: constraints on the timing of the southeastward expansion of the Tibetan Plateau. *Geosci. Front.* 11 (3), 765–781.
- Heinrich, C.A., Eadington, P.J., 1986. Thermodynamic predictions of the hydrothermal chemistry of arsenic, and their significance for the paragenetic sequence of some cassiterite-arsenopyrite-base metal sulfide deposits. *Econ. Geol.* 81: 511–529.
- Heo, C.H., Chung, H.T., Lee, J.H., 2012. Geochemical exploration for REE occurrence in Nghe An Area within Northern Vietnam. *Econ. Environ. Geol.* 45 (6), 599–622.
- Heo, C.H., Ho, T.C., Lee, J.H., 2014. Geochemical exploration for Tri Le REE occurrence in Nghe An Province within Northern Vietnam. *Econ. Environ. Geol.* 47 (2), 147–168.
- Hosking, K.F.G., 1977. Known relationships between the 'hard-rock' tin deposits and the granites of Southeast Asia. *Bull. Geol. Soc. Malays.* 9, 141–157.
- Hou, L., Liu, S., Guo, L., Xiong, F., Li, C., Shi, M., Zhang, Q., Xu, S., Wu, S., 2019. Geology, geochronology, and Hf isotopic composition of the Pha Lek Fe deposit, northern Laos: implications for early Permian subduction-related skarn Fe mineralization in the Truong Son belt. *J. Earth Sci.* 30 (1), 109–120.
- Hu, R.Z., Wei, W.F., Bi, X.W., Peng, J.T., Qi, Y.Q., Wu, L.Y., Chen, Y.W., 2012. Molybdenite Re-Os and muscovite $^{40}\text{Ar}/^{39}\text{Ar}$ dating of the Xihuashan tungsten deposit, central Nanling district, South China. *Lithos* 150, 111–118.
- Hutchison, C., 1984. Geology of tin deposits in Asia and the Pacific, Selected papers from the International Symposium on the Geology of tin deposits, held in Nanning, China, pp. 26–30.
- Jenner, F.E., Holden, P., Mavrogenes, J.A., O'Neill, H.S., Allen, C., 2009. Determination of selenium concentrations in NIST SRM 610, 612, 614 and geological glass reference materials using the electron probe, LA-ICP-MS and SHRIMP II. *Geostand. Geoanal. Res.* 33 (3), 309–317.
- Jolivet, L., Beyssac, O., Goffé, B., Avigad, D., Lepvrier, C., Maluski, H., Thang, T.T., 2001. Oligo-Miocene midcrustal subhorizontal shear zone in Indochina. *Tectonics* 20 (1), 46–57.
- Jolivet, L., Maluski, H., Beyssac, O., Goffé, B., Lepvrier, C., Thi, P.T., Vuong, N.V., 1999. Oligocene-Miocene Bu Khang extensional gneiss dome in Vietnam: geodynamic implications. *Geology* 27 (1), 67.
- Kamvong, T., Khin Zaw, Meffre, S., Maas, R., Stein, H., Lai, C.K., 2014. Adakites in the Truong Son and Loei fold belts, Thailand and Laos: Genesis and implications for geodynamics and metallogeny. *Gondwana Res.* 26 (1), 165–184.
- Kent, A.J.R., 2008. Lead isotope homogeneity of NIST SRM 610 and 612 glass reference materials: Constraints from laser ablation multicollector ICP-MS (LA-MC-ICP-MS) analysis. *Geostand. Geoanal. Res.* 32 (2), 129–147.
- Kent, A.J.R., Jacobsen, B., Peate, D.W., Waught, T.E., Baker, J.A., 2004. Isotope dilution MC-ICP-MS rare earth element analysis of geochemical reference materials NIST SRM 610, NIST SRM 612, NIST SRM 614, BHVO-2G, BHVO-2, BCR-2G, JB-2, WS-E, W-2, AGV-1 and AGV-2. *Geostand. Geoanal. Res.* 28 (3), 417–429.
- Koppers, A.A.P., 2002. ArArCALC—software for $^{40}\text{Ar}/^{39}\text{Ar}$ age calculations. *Comput. Geosci.* 28 (5), 605–619.
- Lacassin, R., Maluski, H., Leloup, P.H., Tappognier, P., Hinthon, C., Siribhakdi, K., Chuaviroj, S., Charoenrat, A., 1997. Tertiary diachronic extrusion and deformation of western Indochina: structural and $^{40}\text{Ar}/^{39}\text{Ar}$ evidence from NW Thailand. *J. Geophys. Res. [Solid Earth]* 102 (B5), 10013–10037.
- Le, V.T., 2015. Characteristics of the Original Tin Mineralization of Suoi Mai Deposit, Quy Hop, Nghe An. Hanoi University of Mining and Geology, Vietnam (in Vietnamese), p. 89. Master's Thesis.
- Lee, J.H., Jin, K.M., Heo, C.H., 2018. REE mineralization of Quy Hop Area in Nghe An Province, Northern Vietnam. *J. Mineral. Soc. Korea* 31 (3), 193–213.
- Lee, J.Y., Marti, K., Severinghaus, J.P., Kawamura, K., Yoo, H.S., Lee, J.B., Kim, J.S., 2006. A redetermination of the isotopic abundances of atmospheric Ar. *Geochim. Cosmochim. Acta* 70 (17), 4507–4512.
- Lehmann, B., 1982. Metallogeny of tin; magmatic differentiation versus geochemical heritage. *Econ. Geol.* 77: 45–59.
- Leloup, P.H., Lacassin, R., Tappognier, P., Schärer, U., Zhong, D., Liu, X., Zhang, L., Ji, S., Trinh, P.T., 1995. The Ailaoshan-Red river shear zone (Yunnan, China), tertiary transform boundary of Indochina. *Tectonophysics* 251 (1–4), 3–84.
- Lepvrier, C., Maluski, H., Vu, V.T., Leyreloup, A., Phan, T.T., Nguyen, V.V., 2004. The early Triassic Indosinian orogeny in Vietnam (Truong Son Belt and Kontum Massif); implications for the geodynamic evolution of Indochina. *Tectonophysics* 393 (1–4), 87–118.
- Lepvrier, C., Maluski, H., Nguyen, V.V., Roques, D., Axente, V., Rangin, C., 1997. Indosinian NW-trending shear zones within the Truong Son belt (Vietnam) $^{40}\text{Ar}/^{39}\text{Ar}$ Triassic ages and Cretaceous to Cenozoic overprints. *Tectonophysics* 283 (1–4), 105–127.
- Li, C.Y., Zhang, R.Q., Ding, X., Ling, M.X., Fan, W.M., Sun, W.D., 2016. Dating cassiterite using laser ablation ICP-MS. *Ore Geol. Rev.* 72, 313–322.
- Lin, J., Liu, Y., Yang, Y., Hu, Z., 2016. Calibration and correction of LA-ICP-MS and LA-MC-ICP-MS analyses for element contents and isotopic ratios. *Solid Earth Sci.* 1 (1), 5–27.
- Liu, J., Chen, X., Wu, W., Tang, Y., Tran, M.D., Nguyen, Q.L., Zhang, Z., Zhao, Z., 2015. New tectono-geochronological constraints on timing of shearing along the Ailaoshan-Red River shear zone: implications for genesis of Ailaoshan gold mineralization. *J. Asian Earth Sci.* 103, 70–86.
- Liu, J., Tang, Y., Tran, M.-D., Cao, S., Zhao, L.I., Zhang, Z., Zhao, Z., Chen, W., 2012b. The nature of the Ailaoshan-Red River (ASRR) shear zone: constraints from structural, microstructural and fabric analyses of metamorphic rocks from the Diancang Shan, Ailaoshan and Day Nui Con Voi massifs. *J. Asian Earth Sci.* 47, 231–251.
- Liu, J., Tran, M.-D., Tang, Y., Nguyen, Q.-L., Tran, T.-H., Wu, W., Chen, J., Zhang, Z., Zhao, Z., 2012a. Permo-Triassic granitoids in the northern part of the Truong Son belt, NW Vietnam: geochronology, geochemistry and tectonic implications. *Gondwana Res.* 22 (2), 628–644.
- Liu, Y., Li, Z., Li, H., Guo, L., Xu, W., Ye, L., Li, C., Pi, D., 2007. U-Pb geochronology of cassiterite and zircon from the Dulong Sn-Zn deposit: Evidence for Cretaceous large-scale granitic magmatism and mineralization events in southeastern Yunnan province, China. *Acta Petrol. Sin.* 23 (5), 967–976.
- Liu, Y., Gao, S., Hu, Z., Gao, C., Zong, K., Wang, D., 2010. Continental and oceanic crust recycling-induced melt-peridotite interactions in the Trans-North China Orogen: U-Pb dating, Hf isotopes and trace elements in zircons from mantle xenoliths. *J. Petrol.* 51 (1–2), 537–571.
- Ludwig, K., 2003. User's manual for a geochronological toolkit for Microsoft Excel (Isoplot/Ex version 3.0). Berkeley Geochronol. Center, Spl. Publ. No 4, 1–71.
- Luu, C.T., Trinh, D.H., Chu, M.T., Dinh, X.H., Nguyen, P., 2020. Some new research outcomes of wolframite-tin-polymetallic metallization in the Huoi Chun area, Huaphanh province, Lao people's democratic republic (LPDR). *J. Min. Earth Sci.* (in Vietnamese with English abstract) 61, 22–32.
- Machado, N., Simonetti, A., 2001. U-Pb dating and Hf isotopic composition of zircon by laser-ablation-MC-ICP-MS. In: Sylvester, P. (Ed.), *Laser Ablation-ICPMS in the Earth sciences: Principles and applications*. Mineralogical Association of Canada, St. John's, Newfoundland, pp. 121–146.
- Manaka, T., Zaw, K., Meffre, S., Vasconcelos, P.M., Golding, S.D., 2014. The Ban Houayxai epithermal Au–Ag deposit in the Northern Lao PDR: Mineralization related to the Early Permian arc magmatism of the Truong Son Fold Belt. *Gondwana Res.* 26 (1), 185–197.
- Mao, W., Zhong, H., Yang, J.H., Tang, Y.W., Liu, L., Fu, Y.Z., Zhang, X.C., Sein, K., Aung, S.M., Li, J., 2020. Combined zircon, molybdenite, and cassiterite geochronology and cassiterite geochemistry of the Kuntabin tin-tungsten deposit in Myanmar. *Econ. Geol.*, 115: 603–625.
- Morley, C.K., 2002. A tectonic model for the Tertiary evolution of strike-slip faults and rift basins in SE Asia. *Tectonophysics* 347 (4), 189–215.
- Moscati, R.J., Neymark, L.A., 2020. U-Pb geochronology of tin deposits associated with the Cornubian Batholith of southwest England: Direct dating of cassiterite by in situ LA-ICPMS. *Miner. Depos.* 55 (1), 1–20.
- Nagy, E.A., Schärer, U., Nguyen, T.M., 2000. Oligo-Miocene granitic magmatism in central Vietnam and implications for continental deformation in Indochina. *Terra Nova* 12 (2), 67–76.
- Nakai, S., Halliday, A.N., Kesler, S.E., Jones, H.D., Kyle, J.R., Lane, T.E., 1993. Rb-Sr dating of sphalerites from Mississippi Valley-type (MVT) ore deposits. *Geochim. Cosmochim. Acta* 57 (2), 417–427.
- Neymark, L.A., Holm-Denoma, C.S., Moscati, R.J., 2018. In situ LA-ICPMS U-Pb dating of cassiterite without a known-age matrix-matched reference material: Examples from worldwide tin deposits spanning the Proterozoic to the Tertiary. *Chem. Geol.* 483, 410–425.
- Nguyen, C.D., Duong, H.S., Bui, D.C., Bui, M.T., 2015. U-Pb zircon SHRIMP isotopic age of Nam Giai granitoid in Phu Hoat (Nghe An) and their geodynamic significance, 50th Anniversary of Vietnam Institute of Geosciences and Mineral Resources, Vietnam Institute of Geosciences and Mineral Resources (in Vietnamese with English abstract), pp. 34–39.
- Nguyen, C.D., Duong, H.S., Nguyen, T.C., Bui, D.C., Nguyen, T.H.T., 2014. Studying Metallogeny and Prospective Division of Mineral Resources in the Phu Hoat Structural Zone. Geological archives, Hanoi (in Vietnamese), p. 145.
- Nguyen, T.A., Yang, X., Vu, T.H., Liu, L., Lee, I., 2019. Piaoac Granites Related W-Sn Mineralization, Northern Vietnam: Evidences from Geochemistry, Zircon Geochronology and Hf Isotopes. *J. Earth Sci.* 30 (1), 52–69.
- Nguyen, V.P., 2012. Report on exploration in the East of Suoi Bac minery, Chau Hong and Chau Thanh commune, Quy Hop district, Nghe An province, Publishing House of Sciences and Technology. Hanoi (in Vietnamese) 93, pp.
- Olade, M.A., 1980. Geochemical characteristics of tin-bearing and tin-barren granites, northern Nigeria. *Econ. Geol.*, 75: 71–82.
- Pearce, N.J.G., Perkins, W.T., Westgate, J.A., Gorton, M.P., Jackson, S.E., Neal, C.R., Chereny, S.P., 1997. A compilation of new and published major and trace element data for NIST SRM 610 and NIST SRM 612 glass reference materials. *Geostand. Newslett.* 21 (1), 115–144.
- Renne, P.R., Balco, G., Ludwig, K.R., Mundil, R., Min, K., 2011. Response to the comment by W.H. Schwarz et al. on "Joint determination of ^{40}K decay constants and $^{40}\text{Ar}^{*}/^{40}\text{Ar}$ for the Fish Canyon sanidine standard, and improved accuracy for $^{40}\text{Ar}/^{39}\text{Ar}$ geochronology" by PR Renne et al. (2010). *Geochim. Cosmochim. Acta* 75, 5097–5100.
- Roger, F., Maluski, H., Lepvrier, C., Vu, V.T., Paquette, J.L., 2012. LA-ICPMS zircons U/Pb dating of Permo-Triassic and Cretaceous magnetisms in Northern Vietnam – Geodynamical implications. *J. Asian Earth Sci.* 48, 72–82.
- Sao, H., 2008. Fluid inclusion characteristics and formation temperatures of granitoid rock, tin-tungsten and gold ore in Vietnam. *J. Geol.* (in Vietnamese) 309, 9–10.
- Schärer, U., Tappognier, P., Lacassin, R., Leloup, P.H., Zhong, D.L., Ji, S.C., 1990. Intraplate tectonics in Asia: a precise age for large-scale Miocene movement along the Ailaoshan-Red River shear zone. *China. Earth Planet. Sci. Lett.* 97, 65–77.
- Schärer, U., Zhang, Lian-Sheng, Tappognier, P., 1994. Duration of strike-slip movements in large shear zones: the Red River belt, China. *Earth Planet. Sci. Lett.* 126 (4), 379–397.
- Searle, M.P., Yeh, M.W., Lin, T.H., Chung, S.L., 2010. Structural constraints on the timing of left-lateral shear along the Red River shear zone in the Ailaoshan and Diancang Shan Ranges, Yunnan, SW China. *Geosphere* 6 (4), 316–338.

- Shi, M.F., Lin, F.C., Fan, W.Y., Deng, Q.i., Cong, F., Tran, M.D., Zhu, H.P., Wang, H., 2015. Zircon U-Pb ages and geochemistry of granitoids in the Truong Son terrane, Vietnam: Tectonic and metallogenic implications. *J. Asian Earth Sci.* 101, 101–120.
- Simonetti, A., Heaman, L.M., Chacko, T., Banerjee, N.R., 2006. In situ petrographic thin section U-Pb dating of zircon, monazite, and titanite using laser ablation-MC-ICP-MS. *Int. J. Mass Spectrom.* 253 (1-2), 87–97.
- Tang, Y., Liu, J., Tran, M.D., Song, Z., Wu, W., Zhang, Z., Zhao, Z., Chen, W., 2013. Timing of left-lateral shearing along the Ailao Shan-Red River shear zone: constraints from zircon U-Pb ages from granitic rocks in the shear zone along the Ailao Shan Range, Western Yunnan, China. *Int. J. Earth. Sci.* 102 (3), 605–626.
- Tappognier, P., Lacassin, R., Leloup, P.H., Schärer, U., Dalai, Z., Haiwei, W.u., Xiaohan, L., Shaocheng, J.i., Lianshang, Z., Jiayou, Z., 1990. The Ailao Shan/Red River metamorphic belt: tertiary left-lateral shear between Indochina and South China. *Nature* 343 (6257), 431–437.
- Taylor, R.G., 1979. *Geology of tin deposits*. Elsevier Scientific Publishing Co, Amsterdam, Netherlands, pp. 1–543 vol. 11.
- Tera, F., Wasserburg, G.J., 1972. U-Th-Pb systematics in three Apollo 14 basalts and the problem of initial Pb in lunar rocks. *Earth Planet. Sci. Lett.* 14 (3), 281–304.
- Tran, H.T., Zaw, K., Halpin, J., Manaka, T., Lee, Y., Hai, L., Hung, D., Hung, N., 2009. Nature of the Phuoc Son-Tam Ky Suture in central Vietnam and implications for gold mineralisation, 10th Biennial SGA Meeting, pp. 963–965.
- Tran, T.V., Faure, M., Nguyen, V.V., Bui, H.H., Fyhn, M.B.W., Nguyen, T.Q., Lepvrier, C., Thomsen, T.B., Tani, K., Charusiri, P., 2020. Neoproterozoic to Early Triassic tectono-stratigraphic evolution of Indochina and adjacent areas: A review with new data. *J. Asian Earth Sci.* 191, 104231.
- Tran, V.T., Nguyen, D.U., Dam, N., 1986. The main tectonic features of Vietnam, Proc. 1st conf. Geol. Indoch, Ho Chi Minh City (in Vietnamese), pp. 363–376.
- Tran, T.H., Tran, T.A., Ngo, T.P., Pham, T.D., Tran, V.A., Izokh, A.E., Borisenco, A.S., Lan, C.Y., Chung, S.L., Lo, C.H., 2008. Permo-Triassic intermediate-felsic magmatism of the Truong Son belt, eastern margin of Indochina. *C. R. Geoscience* 340 (2–3), 112–126.
- Trinh, D.H., Luu, C.T., Nguyen, T.A., Tran, V.A., Phan, H.G., Nagi, T., Boua, L.S., 2021. Paleogene granite magmatism in the north of the Truong Son belt and implication for crustal evolution. *Vietnam J. Earth Sci.* 43, 478–497.
- Trung, N.M., Nuong, N.D., Itaya, T., 2007. Rb-Sr isochron and K-Ar ages of igneous rocks from the Samnua Depression Zone in Northern Vietnam. *J. Mineral. Petrol. Sci.* 102 (2), 86–92.
- Vermeesch, P., 2018. IsoplotR: A free and open toolbox for geochronology. *Geosci. Front.* 9 (5), 1479–1493.
- Wang, S.S., 1983. Age determinations of ^{40}Ar - ^{40}K , ^{40}Ar - ^{39}Ar and radiogenic ^{40}Ar released characteristics on K-Ar geostandards of China. *Sci. Geol. Sin.* (In Chinese with English abstract) 4, 315–323.
- Wang, P.L., Lo, C.H., Lee, T.Y., Chung, S.L., Lan, C.Y., Yem, N.T., 1998. Thermochronological evidence for the movement of the Ailao Shan-Red River shear zone: a perspective from Vietnam. *Geology* 26 (10), 887.
- Wang, X., Yao, X., Wang, S., Zhu, X., Wang, J., Wang, C., 2019. Intraplate extension of the Indochina plate deduced from 26 to 24 Ma A-type granites and tectonic implications. *Int. Geol. Rev.* 61 (14), 1691–1705.
- Wiedenbeck, M., Allé, P., Corfu, F., Griffin, W.L., Meier, M., Oberli, F., Quadtt, A.V., Roddick, J.C., Spiegel, W., 1995. Three natural zircon standards for U-Th-Pb, Lu-Hf, trace element and REE analyses. *Geostand. Newsl.* 19 (1), 1–23.
- Wiedenbeck, M., Hanchar, J.M., Peck, W.H., Sylvester, P., Valley, J., Whitehouse, M., Kronz, A., Morishita, Y., Nasdala, L., Fiebig, J., Franchi, I., Girard, J.P., Greenwood, R.C., Hinton, R., Kita, N., Mason, P.R.D., Norman, M., Ogasawara, M., Piccoli, P.M., Rhede, D., Satoh, H., Schulz-Dobrick, B., Skár, O., Spicuzza, M.J., Terada, K., Tindle, A., Togashi, S., Vennemann, T., Xie, Q., Zheng, Y.F., 2004. Further characterisation of the 91500 zircon crystal. *Geostand. Geoanal. Res.* 28 (1), 9–39.
- Wysocka, A., Świerczewska, A., 2010. Lithofacies and depositional environments of Miocene deposits from tectonically-controlled basins (Red River Fault Zone, northern Vietnam). *J. Asian Earth Sci.* 39 (3), 109–124.
- Xiao, M., Qiu, H.N., Jiang, Y.D., Cai, Y., Bai, X.J., Zhang, W.F., Liu, M., Qin, C.J., 2019. Gas release systematics of mineral-hosted fluid inclusions during stepwise crushing: implications for ^{40}Ar - ^{39}Ar geochronology of hydrothermal fluids. *Geochim. Cosmochim. Acta* 251, 36–55.
- Xu, B., Jiang, S.Y., Wang, R., Ma, L., Zhao, K.D., Yan, X., 2015. Late Cretaceous granites from the giant Dulong Sn-polymetallic ore district in Yunnan Province, South China: Geochronology, geochemistry, mineral chemistry and Nd-Hf isotopic compositions. *Lithos* 218–219, 54–72.
- Xu, L., Bi, X., Hu, R., Zhang, X., Su, W., Qu, W., Hu, Z., Tang, Y., 2012. Relationships between porphyry Cu-Mo mineralization in the Jinshajiang-Red River metallogenic belt and tectonic activity: constraints from zircon U-Pb and molybdenite Re-Os geochronology. *Ore Geol. Rev.* 48, 460–473.
- Yuan, S., Peng, J., Hao, S., Li, H., Geng, J., Zhang, D., 2011. In situ LA-MC-ICP-MS and ID-TIMS U-Pb geochronology of cassiterite in the giant Furong tin deposit, Hunan Province, South China: New constraints on the timing of tin-polymetallic mineralization. *Ore Geol. Rev.* 43 (1), 235–242.
- Yuan, S., Peng, J., Hu, R., Li, H., Shen, N., Zhang, D., 2008. A precise U-Pb age on cassiterite from the Xianghualing tin-polymetallic deposit (Hunan, South China). *Miner. Depos.* 43 (4), 375–382.
- Zack, T., Kooijman, E., 2017. Petrology and geochronology of rutile. *Rev. Mineral. Geochim.* 83, 443–467.
- Khin Zaw, Meffre, S., Lai, C.K., Burrett, C., Santosh, M., Graham, I., Manaka, T., Salam, A., Kamvong, T., Cromie, P., 2014. Tectonics and metallogeny of mainland Southeast Asia—a review and contribution. *Gondwana Res.* 26 (1), 5–30.
- Zhang, D., Zhao, K.D., Wang, B.D., Cheng, K.D., Luo, X.L., Zhang, W., Li, Q., Jiang, S.Y., 2020. Cretaceous granitic magmatism and mineralization in the Shanhу W-Sn ore deposit in the Nanling Range in South China. *Ore Geol. Rev.* 126, 103758.
- Zhang, D., Peng, J., Coulson, I.M., Hou, L., Li, S., 2014. Cassiterite U-Pb and muscovite ^{40}Ar - ^{39}Ar age constraints on the timing of mineralization in the Xuebaoding Sn-W-Be deposit, western China. *Ore Geol. Rev.* 62, 315–322.
- Zhang, L.S., Schärer, U., 1999. Age and origin of magmatism along the Cenozoic Red River shear belt, China. *Contrib. Mineral. Petrol.* 134 (1), 67–85.
- Zhang, R., Lehmann, B., Seltmann, R., Sun, W., Li, C., 2017a. Cassiterite U-Pb geochronology constrains magmatic-hydrothermal evolution in complex evolved granite systems: The classic Erzgebirge tin province (Saxony and Bohemia). *Geology* 45 (12), 1095–1098.
- Zhang, R., Lu, J., Lehmann, B., Li, C., Li, G., Zhang, L., Guo, J., Sun, W., 2017b. Combined zircon and cassiterite U-Pb dating of the Piaotang granite-related tungsten-tin deposit, southern Jiangxi tungsten district, China. *Ore Geol. Rev.* 82, 268–284.
- Zhang, R.Q., Lu, J.J., Wang, R.C., Yang, P., Zhu, J.C., Yao, Y., Gao, J.F., Li, C., Lei, Z.H., Zhang, W.L., Guo, W.M., 2015. Constraints of in situ zircon and cassiterite U-Pb, molybdenite Re-Os and muscovite ^{40}Ar - ^{39}Ar ages on multiple generations of granitic magmatism and related W-Sn mineralization in the Wangxianling area, Nanling Range, South China. *Ore Geol. Rev.* 65, 1021–1042.
- Zhang, S., Zhang, R., Lu, J., Ma, D., Ding, T., Gao, S., Zhang, Q., 2019a. Neoproterozoic tin mineralization in South China: geology and cassiterite U-Pb age of the Baotan tin deposit in northern Guangxi. *Miner. Depos.* 54 (8), 1125–1142.
- Zhang, Z., Xie, G., Mao, J., Liu, W., Olin, P., Li, W., 2019b. Sm-Nd dating and in-situ LA-ICP-MS trace element analyses of scheelite from the Longshan Sb-Au deposit, Xiangzhong metallogenic Province, South China. *Minerals* 9 (2), 87. <https://doi.org/10.3390/min9020087>.
- Zong, K., Chen, J., Hu, Z., Liu, Y., Li, M., Fan, H., Meng, Y., 2015. In-situ U-Pb dating of uraninite by fs-LA-ICP-MS. *Sci. China Earth Sci.* 58 (10), 1731–1740.
- Zong, K., Klemd, R., Yuan, Y.u., He, Z., Guo, J., Shi, X., Liu, Y., Hu, Z., Zhang, Z., 2017. The assembly of Rodinia: the correlation of early Neoproterozoic (ca. 900 Ma) high-grade metamorphism and continental arc formation in the southern Beishan Orogen, southern Central Asian Orogenic Belt (CAOB). *Precambrian Res.* 290, 32–48.